HOKKAIDO UNIVERSITY

Title	Preparation of lignin-based activated carbon fibers and their application to electrodes for electric double layer capacitor
Author(s)	游, 翔宇
Degree Grantor	北海道大学
Degree Name	博士(農学)
Dissertation Number	甲第12438号
Issue Date	2016-09-26
DOI	https://doi.org/10.14943/doctoral.k12438
Doc URL	https://hdl.handle.net/2115/67172
Type	doctoral thesis
File Information	Xiangyu_You.pdf

Hokkaido University Collection of Scholarly and Academic Papers : HUSCAP

Preparation of lignin-based activated carbon fibers and their application to electrodes for electric double layer capacitor

(リグニンを原料とする活性炭素繊維の調製と電気二重層キャパシタ用電極への応用)

Xiangyu You

Doctoral thesis

Supervisor: Professor Yasumitsu Uraki

Laboratory of Forest Chemistry
Division of Environmental Resources
Graduate School of Agriculture
Hokkaido University

Sapporo

September 2016

Contents

Contents ..... **i**

Abbreviations list ..... **iii**

Chapter 1 Introduction **1**

1.1 Motivation for conversion of isolated lignin into value-added materials 1

1.2 Lignin and its isolation method 5

1.3 Preparation of lignin based ACFs 8

1.3.1 Electrospinning 9

1.3.2 Melt spinning 11

1.4 Electric double layer capacitors (EDLCs) 12

1.5 Research objectives 16

Chapter 2 Preparation of ACFs from electrospun and melt-spun lignin fibers **18**

2.1 Introduction 18

2.2 Experimental 18

2.2.1 Isolation of lignin 19

2.2.2 Electrospinning of HAL and its thermostabilization 22

2.2.3 Electrospinning of PEGL and its thermostabilization 23

2.2.4 Electrospinning of SL and its thermostabilization 24

2.2.5 Melt spinning of PEGL and its chemical thermostabilization 24

2.2.6 Carbonization 25

2.2.7 Steam activation 25

2.2.8 Characterization 26

2.3. Results and discussion 28

2.3.1 ACFs from electrospun HAL fibers 28

2.2.2 ACFs from Electrospun PEGL fibers 34

2.3.3 ACFs from electrospun SL fibers 37

2.3.4 ACFs from melt spun PEGL fibers 39

2.2.5 Surface area and pore size distribution 41

Chapter 3 Single cell type electric double layer capacitors (SC-EDLCs) assembly and their electrochemical performance by using different electrolytes 46

3.1 Introduction 46

3.2 Experimental 47

3.2.1 Materials 47

3.2.2 Electrolyte preparation 47

3.2.2 Electrodes preparation 48

3.2.3 SC-EDLC assembly 49

3.2.4 Characterization 50

3.3 Results and discussion 55

3.3.1 Electrochemical properties of SC-EDLCs with organic electrolyte 55

3.3.2 Electrochemical properties of SC-EDLCs with aqueous electrolyte 65

Chapter 4 Internal tandem electric double layer capacitors (IT-EDLCs) assembly and characterization of their electrochemical performance 70

4.1 Introduction 70

4.2 Experimental 71

4.2.1 Materials 71

4.1.2 Electrode preparation 71

4.1.3 IT-EDLC assembly 73

4.1.4 Characterization 73

4.3 Results and discussion 75

4.3.1 IT-EDLC in series connection 75

4.2.2 IT-EDLC in parallel connection 79

4.2.3 IT-EDLC in S/P comb. connection 81

Chapter 5 Conclusions 84

References 89

Acknowledgements 98

Abbreviations list

AC	Activate charcoal
ACF(s)	Activate carbon fiber(s)
AL	Acetic acid lignin
BET	Brunauer, Emmett, and Teller
CB	Carbon black
CF(s)	Carbon fiber(s)
CMC	Carboxymethyl cellulose sodium
CV	Cyclic voltammetry
DH	Dollimore Heal
DMF	Dimethylformamide
EDLC(s)	Electric double layer capacitor(s)
$EDLC_{AC\ powder}$	EDLC assembled with AC powder as electrode constituent
$EDLC_{E\text{-}HAL\text{-}ACF\text{-}105/180}$	EDLC assembled with E-HAL-ACF-105/180 as electrode constituent
$EDLC_{E\text{-}PEGL\text{-}ACF\text{-}105/180}$	EDLC assembled with E-PEGL-ACF-105/180 as electrode constituent
$EDLC_{E\text{-}SL\text{-}ACF\text{-}180}$	EDLC assembled with E-SL-ACF-180 as electrode constituent
$EDLC_{M\text{-}PEGL\text{-}ACF\text{-}105/180}$	EDLC assembled with M-PEGL-ACF-105/180 as electrode constituent
E-HAL-ACF	Activated carbon fibers derived from electrospun HAL fibers
E-HAL-ACF-105/180	Activated carbon fibers derived from electrospun HAL fibers comsuming 105/180 mL of H_2O for activation
E-HAL-CF	Carbon fibers derived from electrospun HAL fibers
EIS	Electrochemical impedance spectroscopy
E-PEGL-ACF-105/180	Activated carbon fibers derived from electrospun PEGL fibers comsuming 105/180 mL of H_2O for activation

E-SL-ACF-180	Activated carbon fibers derived from electrospun SL fibers comsuming 180 mL of H_2O for activation
E-SL-CF	Carbon fibers derived from electrospun SL fibers
GCD	Galvanostatic charge and discharge
HAL	Hardwood acetic acid lignin
Hexamine	Hexamethylenetetramine
IT-EDLC(s)	Internal tandem electric double layer capacitor(s)
$IT\text{-}EDLC_{AC\ powder}$	IT-EDLC assembled with AC powder as electrode constituent
$IT\text{-}EDLC_{M\text{-}PEGL\text{-}ACF\text{-}105/180}$	IT-EDLC assembled with M-PEGL-ACF-105/180 as electrode constituent
M-PEGL-ACF-105/180	Activated carbon fibers derived from melt spun PEGL fibers comsuming 105/180 mL of H_2O for activation
PAN	Polyacrylonitrile
PC	Propylene carbonate
PE	Polyethylene
PEG	Polyethylene glycol
PEGL	Polyethylene glycol lignin
PTFE	Polytetrafluoroethylene
S/P comb.	Series/parallel combination
SAL	Softwood acetic acid lignin
SC-EDLC(s)	Single cell type electric double layer capacitor(s)
$SC\text{-}EDLC_{M\text{-}PEGL\text{-}ACF\text{-}105/180}$	SC-EDLC assembled with M-PEGL-ACF-105/180 as electrode constituent
SEM	Scanning electron microscope

Chapter 1 Introduction

1.1 Motivation for conversion of isolated lignin into value-added materials

There is an urgency to develop bio-based products and innovative technologies that can reduce widespread dependence on fossil resources(Bozell and Petersen, 2010). Cellulose and lignin are the most and second abundant components of plant biomass, respectively. Lignin as a by-product of pulp and paper industry is mainly burned for energy recovery (Calvo-Flores and Dobado, 2010). For sustainable production processes based on renewable woody biomass, lignin utilization is one of the key technology not only for energetic purposes but also as for material use as chemicals and plastics. To accelerate lignin utilization, production of value-added material from lignin is also an important subject.

Current applications of lignin are dispersants, emulsion stabilizers, surfactants, and binders, which are mostly made from ligninsulfonates (Mathiasson and Kubat, 1994; Calvo-Flores and Dobado, 2010). Homma et al. developed lignin amphiphiles with high surface activity (Homma et al., 2010) and Aso et al. proved them to be superior cement dispersant to ligninsulfonates (Aso et al., 2013). Besides, lignin can be used as a reactant to synthesize polymers or resins, such as phenol-formaldehyde resins, polyester, polyurethanes and etc., in addition to an additives or bulking fillers for synthetic polymers (Ciobanu et al., 2004; Pouteau et al., 2004; Gandini, 2008; Stewart, 2008; Binh et al., 2009). However, these are not high value-added materials from lignin. The lack of its value-added application is due to the fact that lignin is

composed of heterogeneous monolignols, and its structure is very complicated, and its physicochemical properties are varied by isolation process.

Carbonaceous materials are being highly focused on as one of the value-added functional materials. One is carbon fibers (CFs), which are employed as CF-reinforced composites in wide areas, such as sports equipment, construction, aircraft and automotive industries, because of high strength and lightweight (Kadla et al., 2002; Baker et al., 2012; Frank et al., 2012). Commercial CFs are produced mainly from two types of raw materials, pitch of petroleum or coal, and polyacrylonitrile (PAN). Lignin is also considered as an alternative resource for CFs production, because it is rich in carbon among wood components, and is considered as a cheap material (about US $150 / ton) (Voitl and Rohr, 2009). Several CFs produced from isolated lignins were reported so far (Sudo and Shimizu, 1992; Uraki et al., 1995; Kadla et al., 2002; Kubo and Kadla, 2004; Kubo and Kadla, 2005). However, the stiffness and tensile strength of the reported CFs were inferior to those of commercial ones. So the mechanical properties of lignin-based CFs should be further improved to meet the conventional industry requirements (Frank et al., 2012).

Activated carbon fibers (ACFs) are one of the further functionalized CFs. ACFs are highly porous material, and have drawn much attention as an adsorption material. ACFs are produced by gas and chemical activations of CFs. Uraki et al. prepared ACFs from softwood acetic acid lignin (SAL) (Uraki et al., 2001). The ACFs possessed a large specific surface area of 1930 m^2/g, and had adsorption ability comparable to that of high-performance commercial ACFs. The tensile strength was

also comparable to that of pitch-derived ACFs.

Electric double layer capacitor (EDLC) is a kind of energy storage devices as well as conventional capacitor and secondary battery, such as lithium ion battery. EDLC has several advantages over the secondary battery, such as (1) high power density (discharge at high current density), (2) short time needed for full charging, (3) long cycle life due to no chemical reactions, (4) high coulombic efficiency (high reversibility), and (5) environmental friendliness (no heavy metals used), even though its energy density is lower than secondary battery (Inagaki et al., 2010). Therefore, EDLC has been considered to be a next-generation energy storage device to meet the increasing demands of electric power (**Figure 1**) (Simon and Gogotsi, 2008). EDLC consists of three parts: electrode, electrolyte and separator. Carbonaceous materials are considered as prospective electrode materials for industrialization. The advantages of carbon materials over other candidates for the electrode are abundance, lower price, easy processing, non-toxicity, high specific surface area, good electronic conductivity, high chemical stability, and wide operating temperature range (Wang et al., 2012). In addition, adsorption occurs much faster at the larger surface of ACFs than at the surface of commercial activated charcoal (AC).

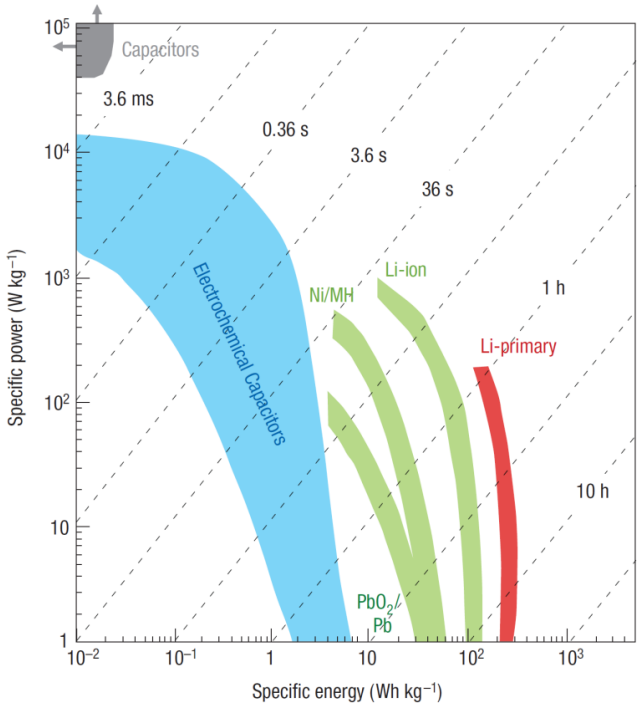

Figure 1. Ragone plot showing the specific power against specific energy for various electrical energy storage systems. If a supercapacitor is used in an electric vehicle, the specific power shows how fast one can go, and the specific energy shows how far one can go on a single charge. Times shown are the time constants of the devices, obtained by dividing the energy density by the power (Simon and Gogotsi, 2008)

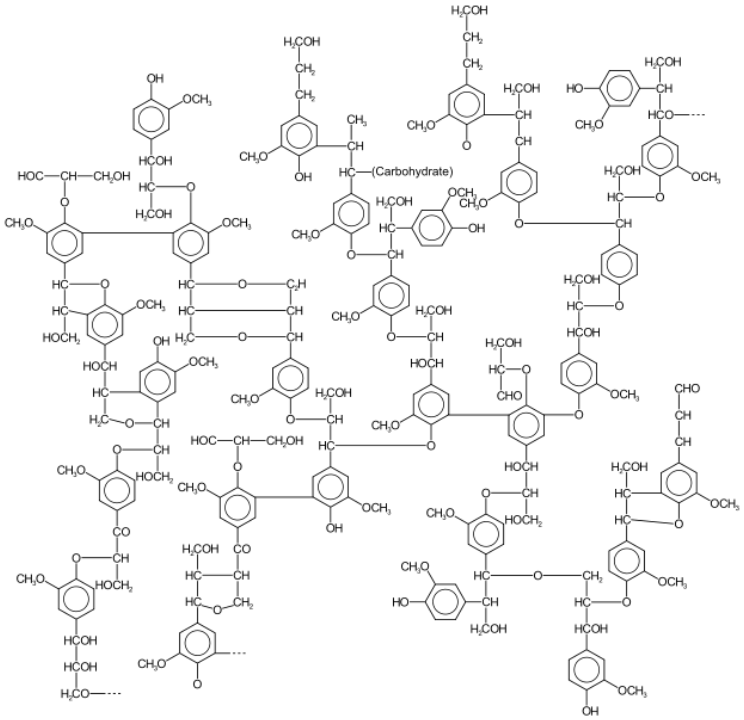

Figure 2. A suggested structure of lignin (Wikipedia contributors, 2016b)

It is because the physical adsorption on ACFs directly occurs on the surface but not inside the fibers; whereas adsorbates first diffuse into inside of commercial AC through the macropores, and then packed into the micropores (Uraki et al., 1997). Since pure electrostatic charge accumulates at the electrode/electrolyte interface of EDLC, the electrostatic capacitance of EDLC is strongly dependent on the surface area of the electrode (Zhang and Zhao, 2009). Accordingly, ACFs with large surface area is suitable material for electrode of EDLC.

In this chapter, I further introduce more details on lignin, ACFs production and EDLC assembly as follows.

1.2 Lignin and its isolation method

Lignin is a complex polymer that exists predominantly in the xylem of many plants, and accounts for 20–30% of the whole wood components. A proposed structure of lignin is shown in **Figure 2**. Lignin seems to contribute to rigidity of reinforce wood cell wall, to protection against pathogens, and water transportation system in tree. The structure of lignins varies depending on the plant source, i.e. softwood, hardwood, grasses, and the tissue in plant, i.e. branch and stem, and the methods of isolation. The degree of polymerization in native lignin is not known, since it is inevitably fragmented during extraction, but is believed to be very high (Gellerstedt and Henriksson, 2008; Calvo-Flores and Dobado, 2010).

There are three precursors or monolignols, *p*-coumaryl alcohol, coniferyl

alcohol, and sinapyl alcohol, which are polymerized by the action of enzyme, oxidase and/or peroxidase. The chemical structures of monolignols are depicted in **Figure 3** (Calvo-Flores and Dobado, 2010). The aromatic structure of each monolignol is referred to as *p*-hydroxyphenyl (H), guaiacyl (G), and syringyl (S), respectively. Softwoods lignin consists mostly of G-units and a trace amount of H-units, while hardwoods lignin is generally made of G and S structures in addition to a small amount of H unit.

The most frequent interunitary linkage in lignin is a β–O–4 bond, which occupies about 50% of the linkages in softwoods and about 60% in hardwoods. Therefore, chemical pulping to separate lignin from the carbohydrate components is performed to cleave this linkage for lignin dissolution. The second abundant interunitary linkage is a 5-5 linkage (20% in softwood and 9% in hardwoods). Other linkages, such as β–5, 4–O-5, and β-β, are observed in softwood at a lower frequency (**Figure 4**).

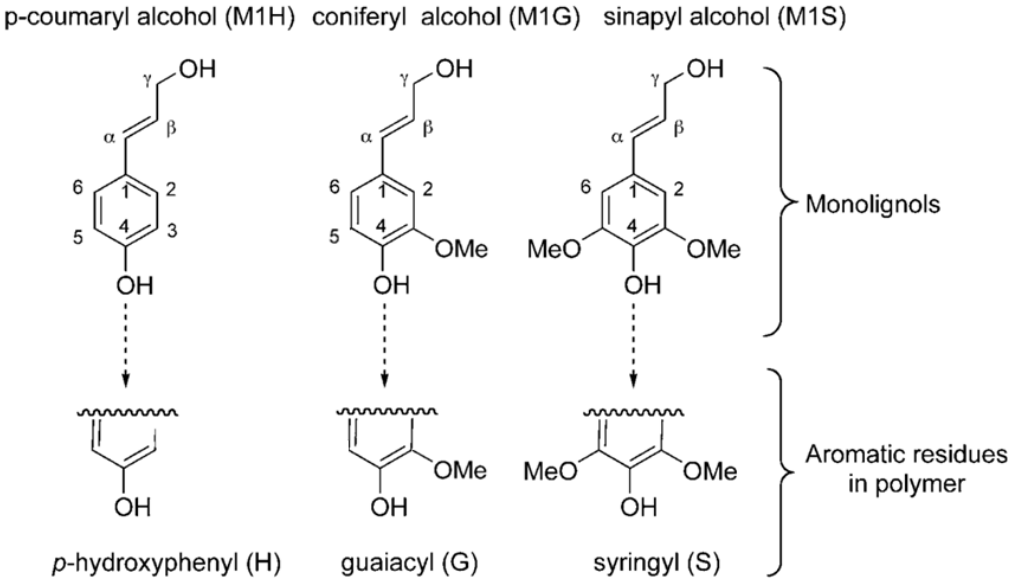

Figure 3. Monolignol carbon nomenclature and residues

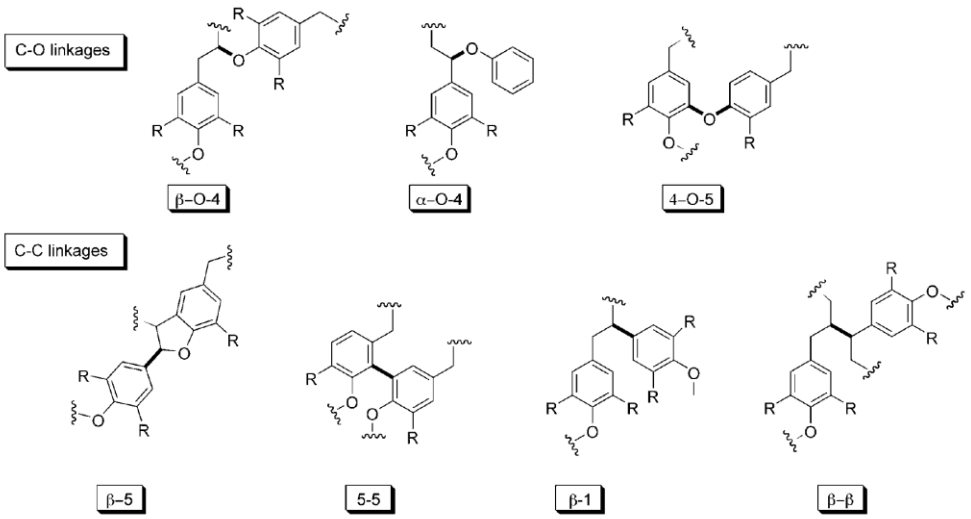

Figure 4. C-O and C-C linkages between monolignols

Lignin can be isolated by different pulping methods, whose chemical properties depend on the isolation method. Organosolv pulpings are carried out by using organic solvents as a cooking solvent, such as methanol, ethanol, polyethylene glycol (PEG) and organic acids together with or without catalysts at cooking temperatures between120 to 250 ^{o}C (Johansson et al., 1987). By the pulpings, interunitary linkages of lignin are cleaved, and accordingly lignin fragments are dissolved in cooking solvents. So-called organosolv lignin as a solid form can be obtained by precipitation with water from the cooking black liquor (Kaneko, 1994). In this study, I used two kinds of organic lignins, acetic acid lignin (AL) and polyethylene glycol lignin (PEGL).

In the case of AL, hydroxyl groups in AL were partially acetylated in acetic

acid wih an aid of acid catalyst during the acetic acid pulping. The acetyl content was 8.4% on lignin (Kubo et al., 1998). Of course, this AL dissolves in acetic acid. This property is very important for the following electrospinning.

According to previous studies, PEGL showed fusibility due to its PEG moieties introduced into the lignin during the pulping process (Lin et al., 2012). The PEG content was around 40-50% on lignin (Lin et al., 2012; Lin et al., 2013). Thereby, this PEGL dissolves in organic solvents, such as acetic acid. The fusibility and solubility in organic solvent of PEGL are also important for the ACFs preparation.

Soda pulping is a conventional pulping method with sodium hydroxide as the cooking chemical. This pulping method is very popular, especially in China (Jiang et al., 1991; Montane et al., 1998; Rodr ́guez et al., 2008). So far, the soda puling has been well studied as a delignification process for bioethanol production using cedar wood via enzymatic saccharification by Forestry and Forest Products Research Institute, Tsukuba, Japan (Gosselink et al., 2004). The resultant lignin, soda lignin (SL), shows higher amount of phenolic hydroxyl groups than that from ethanol pulping and formic acid pulping, which indicates that SL is a more reactive material than other lignins (Mansouri et al., 2007).

1.3 Preparation of lignin based ACFs

ACFs can be prepared from lignin fibers as precursor by thermostabilization, carbonization and subsequent activation. To avoid melting of fibers during carbonization, thermostabilization is carried out before carbonization at 200-300 ^{o}C in

air or oxsygen (Braun et al., 2005). The following carbonization is carried out at 1000-3000 ^{o}C under an inert atmosphere, such as nitrogen or argon (Chand, 2000). Finally, CFs can be further converted to ACFs with large specific surface area by activation (Uraki et al., 2001).

So far, lignin fibers can be obtained by several spinning methods, such as electrospinning and melt-spinning.

1.3.1 Electrospinning

Electrospinning is a method to produce very fine fibers with diameters of nano- to micrometer order from synthetic and natural polymers (Norris et al., 2000; Matthews et al., 2002; Ko et al., 2003; Gupta et al., 2005; Li et al., 2005; Dallmeyer et al., 2010). Electrospinning machine basically consists of three components, a high voltage supplier, a nozzle with a small diameter, and a metal collector, as shown in **Figure 5**. In our lab machine, a syringe is used as a nozzle, and is filled with a polymer solution. An electrode of power supplier is connected to a needle part of the syringe, while the metallic collector is connected to ground. By electric charging, the body of the liquid becomes charged, and electrostatic repulsion counteracts the surface tension and the droplet is stretched. At a critical point, a stream of liquid erupts from the surface. This point of eruption is known as the Taylor cone. When the electric force is beyond this critical point, this cone is unstable and a jet of fluid is emitted from the tip of the cone. Due to the potential difference between the nozzle tip and the collector, the solution jet is stretched by electric force, whipped and flew

toward the collector. During this process, the jet diameter is being decreased before the solution jet is totally dried by air. As a result, the solution jet transformed to fibers, and the fibers deposit on the collector.

A reduction of the fiber diameter increases the surface-to-volume ratios of the fibers. From this viewpoint, electrospun nanofibers have been applied to many fields, such as composite reinforcement, filtration, tissue engineering, electronics, drug delivery, wound healing, nanosensors and etc (Tsai et al., 2002; Huang et al., 2003; Ayutsede et al., 2005; Pham et al., 2006; Chen et al., 2008). Electrospinning can also be applied for a wide variety of polymers to produce highly porous nonwoven fabrics.

Many processing parameters have been reported to affect electrospinability and properties of electrospun fibers (Huang et al., 2003; Ramakrishna et al., 2005; Reneker and Yarin, 2008), which include: polymer itself, i.e. molecular weight, molecular weight distribution, structure of the polymer; solution properties such as viscosity, conductivity; spinning parameters, i.e. distance between the capillary and the collector, and motion of the collector; and ambient parameters, including temperature and humidity (Beachley and Wen, 2009).

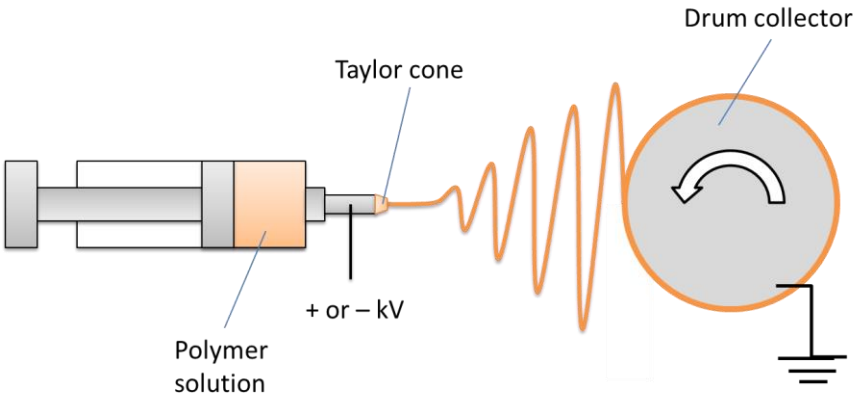

Figure 5. Diagram of fibers formation by electrospinning

1.3.2 Melt spinning

Melt-spinning is an effective method for fast production of polymeric fibers with low cost, because only heat is required during this process. It uses heat to melt the polymer and extrudes the polymer fluid through a spinneret to obtain the fibers by solidification.

A typical melt-spinning scheme is shown in **Figure 6**. Polymer melts are pressed by pressure device through a metal spinneret containing small holes, and converted to thin strands. Then, these strands are cooled and solidified by air, and collected on a roller.

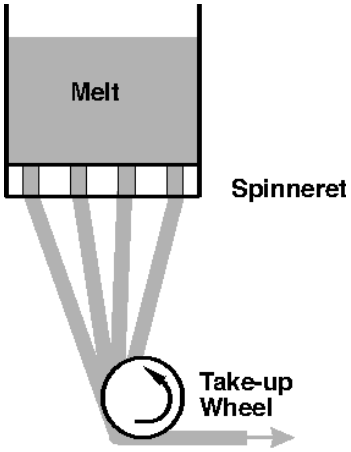

Figure 6. A Schematic image of melt spinning process

Lignin-based fibers by melt-spinning have already been fabricated successfully by using acetic acid lignin and Kraft lignin (Uraki, Y. et al., 1995; Norberg, I. et al., 2012).

1.4 Electric double layer capacitors (EDLCs)

Although the formation of electric double layer had been discovered in 1879 by Helmholtz, development of EDLC as an electric energy storage device is comparatively new (Simon and Gogotsi, 2008; Inagaki et al., 2010; You et al., 2015a; You et al., 2015b). **Figure 7** shows the image model for the formation of electric double layer at the electrolyte/electrode interface. In the charge process, a power supply is directly connected to two electrodes of EDLC and creates potential difference immediately between them. Meanwhile, the electrolyte ions as inductive charges are starting with moving towards the electrodes with opposite polarity. The accumulated electrolyte ions can finally form two equal electric equivalent layers (named as electric double layer) with each electrode until it is fully charged. When the power supply is replaced to an electric resistance, discharge process is occurred. The electrons transfer proceeds from negative electrode to positive one continuously (to form current in the external circuit) until the potential difference become zero. Simultaneously, electrolyte ions are gradually released from electrode, and reach charge balance in the end. By contrast, conventional capacitor can form just one layer during charge and discharge processes, because only inductive charge exists on the electrode. In addition, the charge storage in EDLC is donated by non-faradic adsorption (without redox reactions) at the surface of electrodes and the following theoretical formula,

Charge process

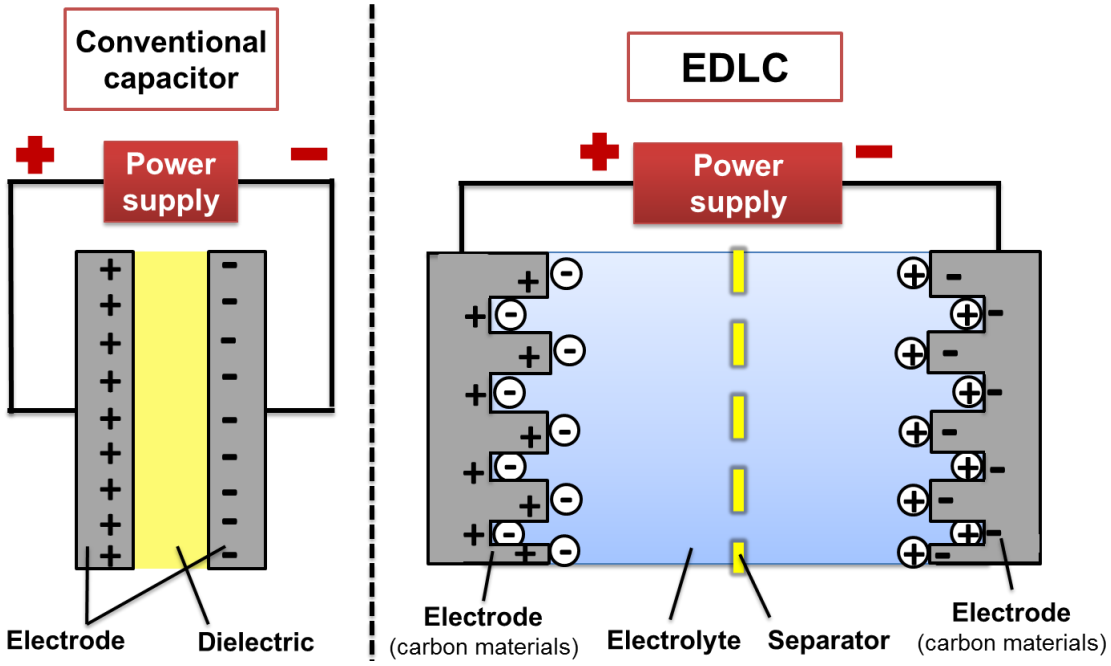

Discharge process

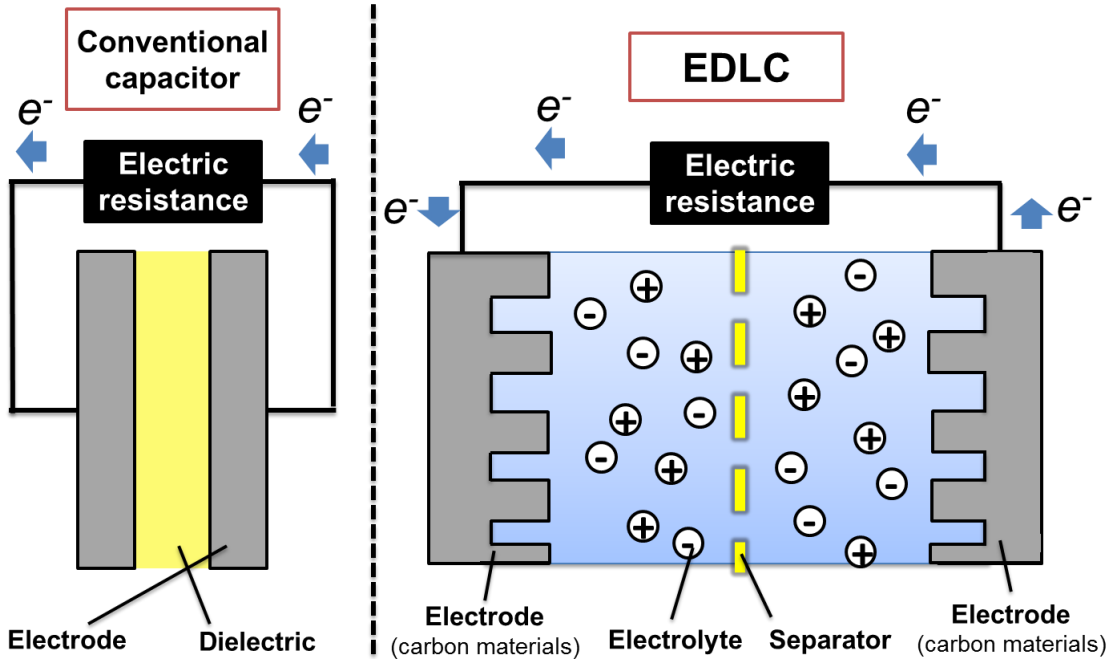

Figure 7. Formations of electric double layer in an EDLC and single layer in a conventional capacitor

$$C = \int \varepsilon \, ds / 4\pi\delta = k \times s \quad (1)$$

shows that the capacitance (C) is dependant on the effective surface (s) because the dielectric constant(ε) and the distance from the surface of electrode to electrolyte ion (δ) are constant in EDLC. (Shi, 1996; Salitra et al., 2000; Gryglewicz et al., 2005).

The performance of an EDLC is not only dependent on the electrode materials, but is also strongly affected by the electrolytes employed. A high EDLC-operating voltage provides both high energy density (the amount of energy stored in the EDLC, in Wh kg^{-1}) and power density (the storage rate of a certain amount of energy in the EDLC, in W kg^{-1}) according to the following equations:

$$E = \frac{1}{8} C V_{max}^2$$

where E is energy density, C is the specific capacitance based on weight of electrode material, and V_{max} is the maximum value of the operating potential range of EDLCs.

$$P = \frac{E}{t}$$

where P is power density, and t is the discharge time.

Therefore, the EDLC performance is limited by the stability of the electrolyte in the applied potential. Current studies of electrolytes involves not only aqueous electrolyte, which has a low operating voltage of 1 V (due to the thermodynamic decomposition of water), but also non-aqueous medium which allows a higher voltage window of about 3 V (Zhang and Zhao, 2009). The most recent EDLCs available in the market use electrolytes based on organic solvents, typically acetonitrile or carbonate-based solvents (i.e. propylene carbonate). These EDLCs achieve a higher

energy density when using organic electrolyte rather than aqueous electrolyte. However, there are other concerns for the use of non-aqueous electrolytes such as high cost, low conductivity compared to aqueous electrolyte leading to power deterioration, low dielectric constant resulting in smaller capacitance, complex purification procedure as well as safety concerns due to the flammability and toxicity of the organic solvent (Zhang and Zhao, 2009).

In order to achieve high operating voltage and energy density that is required by many power devices in practice, another simple and effective approach is to optimize the device configuration, which can be realized by using the tandem architecture. Normally, single cell type EDLC (SC-EDLC) devices, which contain one pair of electrode and one piece of separator in each device, are packed in modules by externally series-connection (**Figure 8**) to obtain a high working voltage (Chen et al., 2015). Although the high operating voltage is achieved by using this method, the weight and volume of such modules is largely increased and the energy density is decreased due to the extra connection parts. To overcome this problem, internal tandem EDLCs (IT-EDLCs) system including two or more pairs of active electrodes with more separators in one device is established.

Figure 8. Externally connected EDLCs

To our knowledge, series-connected IT-EDLCs have been reported (Zhang et al., 2014; Chen et al., 2015). Such IT-EDLCs greatly increase the working voltage in one packaged device and also reduce the packaging cost which generally takes a significant weight fraction (>60%) of the whole cell. However, there are little research concerning about parallel and S/P comb. connections, which result in large total electrostatic capacitance and energy density. The lack of study in this area might be caused by the complex inner structure of IT-EDLC in these two connections, where short circuit easily happens and results in a decrease in performance decrease. Therefore, in addition to the series connection, the parallel and series/parallel combination (S/P comb.) electrode connections still need to be investigated, and the electrochemical performance of the resultant IT-EDLCs should be analyzed.

1.5 Research objectives

The main objectives of this study are 1) to prepare lignin-based activated carbon fiber from AL, PEGL and SL, 2) to assemble SC-EDLC with resultant carbon materials with different electrolytes, and 3) to obtain IT-EDLC with high

electrochemical performance by using internal tandem architecture.

To achieve objective 1, electrospinning and melt-spinning are chosen for AL and PEGL. Both lignins can be dissolved in acetic acid, which is a suitable solvent for electrospinning. So thinner fibers are expected to be easily obtained. In addition, melt spun PEGL fibers are also prepared due to the good fusibility of PEGL (Lin et al., 2012; Lin et al., 2013). On the other hand, SL as a commercially available technical lignin shows high amount of hydroxyl group (Mansouri and Salvadó, 2006), and is expected to be dissolved in solvents, making it suitable for electrospinning. These results are described in Chapter 2.

SC-EDLC assembly is described in Chapter 3. In this chapter, the resultant ACFs are employed as electrode materials. Additionally, Both aqueous and organic electrolyte solution are used in the assembly process. Especially, electrochemical properties of assembled SC-EDLCs will be further discussed.

In Chapter 4, melt spun PEGL fibers are used as an electrode material to assemble IT-EDLC. Three types of IT-EDLCs in series, parallel and S/P comb. are introduced here. The details of preparation method and the electrochemical performance will be further investigated.

Chapter 2 Preparation of ACFs from electrospun and melt-spun lignin fibers

2.1 Introduction

ACFs preparation is an initial step of lignin application in EDLC. ACFs have been on market since 1960s, and they can be made from fiber-form precursors by thermostabilization and subsequent carbonization and activation (Suzuki, 1994). Currently, the major precursors for producing ACF are polyacrylonitrile (PAN), novoloid (novolac resin) and viscose rayon fibers, etc (Jieying et al., 2014). Lignin has also been reported as one of the prospective bioresources for ACFs production (Uraki et al., 1997; Uraki et al., 2001).

In this chapter, I report the preparation of lignin fibers from HAL, PEGL, and SL as precursors for CFs and ACFs by using electrospinning and melt spinning. The morphology (fiber diameter and pores), surface area, pore size distribution, and average pore diameter, are mainly measured to characterize the fibers.

2.2 Experimental

White birch (*Betura Platyphylla* Sukatchev var. *japonica* Hara) wood chips were obtained from Uryu Experimental Forest. Cedar wood chips and SL were supplied by the Department of Biomass Chemistry in Forestry and Forest Products Research Institute (FFPRI), Tsukuba, Ibaraki, Japan. PEG 400 was purchased from Nacalai Tesque. Inc. (Kyoto, Japan). Commercial activated charcoal powder (AC powder), PEG 500,000, acetic acid (AcOH), carbon tetrachloride (CCl_4), dimethylformamide

(DMF), H_2SO_4, NaOH and hexamethylenetetramine (hexamine) were purchased from Wako Pure Chemical Industries, Co., Ltd., Japan. All chemicals were used as received without further purification.

2.2.1 Isolation of lignin

2.2.1.1 Isolation of hardwood acetic acid lignin (HAL)

A preparation scheme of HAL is shown in **Figure 9**. Birch wood chips (258.3 g on oven-dry weight basis) were placed in a round-bottom flask together with 1.292 L of 90 % aqueous acetic acid, and refluxed for 1 h. Then, 3.52 ml of 72% H_2SO_4 (0.32 wt% on aqueous AcOH) was added to the suspension, and the liquor was refluxed for further as a cooking process. At the end of cooking, 63 ml of 2 mol L^{-1} aqueous NaOH solution (1.5 times of H_2SO_4) was added to the flask to neutralize the H_2SO_4.

After cooling the flask to room temperature, the resultant mixture was filtrated through filter paper (No.5C, Advantec), and the residue was washed with 90% AcOH (ca. 500 mL) for 3 times. The filtrate and washings were combined, and concentrated by evaporation under reduced pressure to about 1/5 the volume of the original. The concentrated liquor was slowly poured into 4 L of distilled water with stirring. The precipitate (lignin) was collected by vacuum filtration, and washed with 1 L of distilled water (60 ^{o}C) at least 3 times until the filtrate became clear or nearly colorless. Finally, HAL powder was obtained by freeze drying.

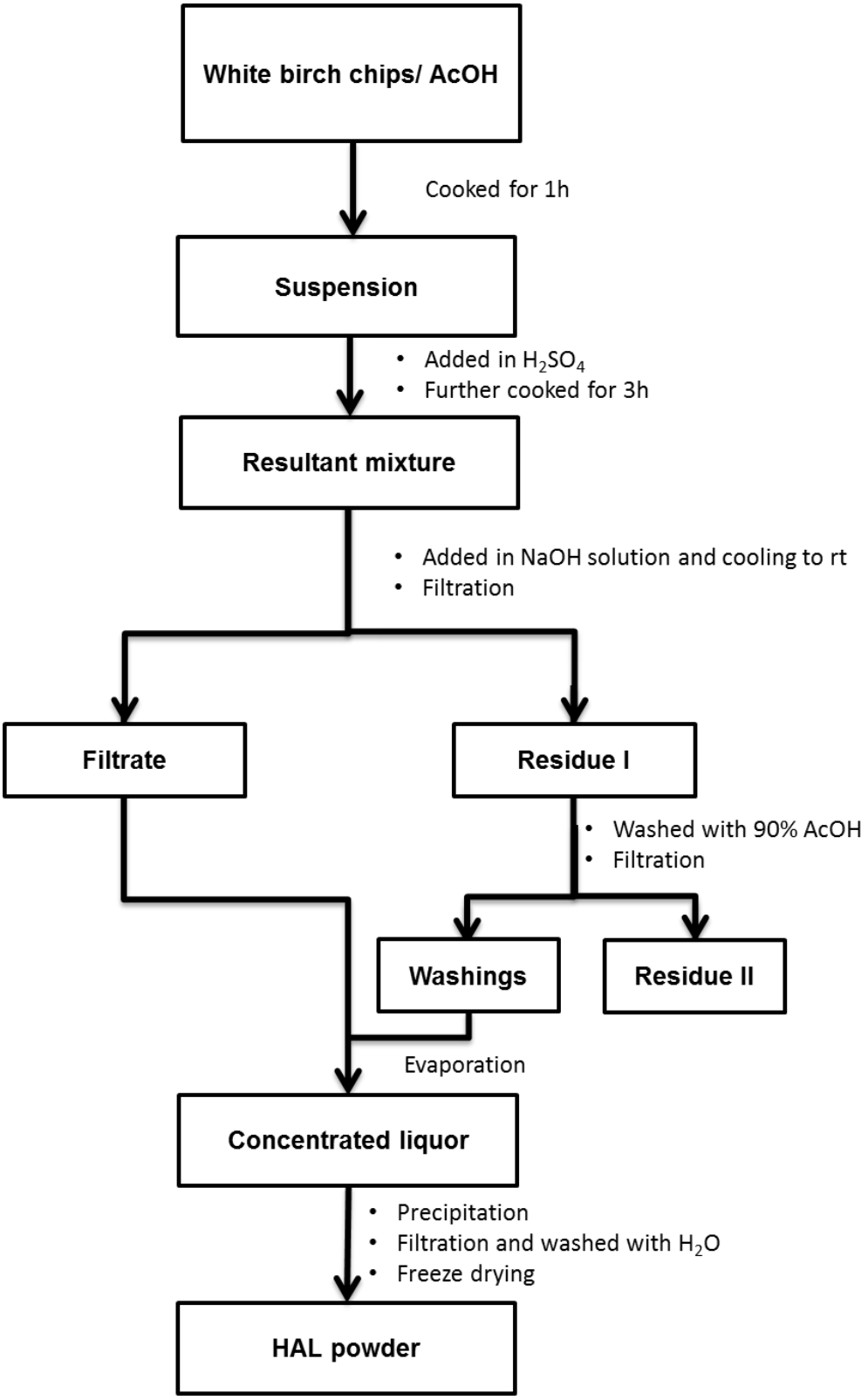

Figure 9. Preparation scheme of HAL

2.2.1.2 Isolation of PEGL

PEGL was isolated from cedar chips by a solvolysis pulping using polyethylene glycol (PEG) 400. The experimental scheme is shown in **Figure 10**. Sixty gram of cedar chips (dry weight) and 300 g of PEG 400, together with 0.9 g of 95 % aqueous H_2SO_4 (0.3 wt% of H_2SO_4 on PEG 400) as an acid catalyst, were placed in a round bottom flask. The flask was first immersed in an oil bath at 160 ℃, kept standing for 240 min. Then, the flask was cooled to room temperature with ice water, and 1.2 L of 80 % 1,4-dioxane aqueous solution was added to the reaction mixture. Afterwards, the resultant mixture was filtrated with filter paper (No.5C, Advantec).

The 1,4-dioxane in the filtrate was removed by evaporation under reduced pressure. The residual liquor (aqueous suspension) was transferred to a three-neck flask equipped with a mechanical stirrer and a thermocouple. The liquor was heated at 140 ℃ for 150 min. After cooling of the flask, 4 L of distilled water was poured into the mixture with stirring for 30 min, to precipitate lignin. After centrifugation (11600 G for 15 min) and freeze-drying, PEGL powders were obtained.

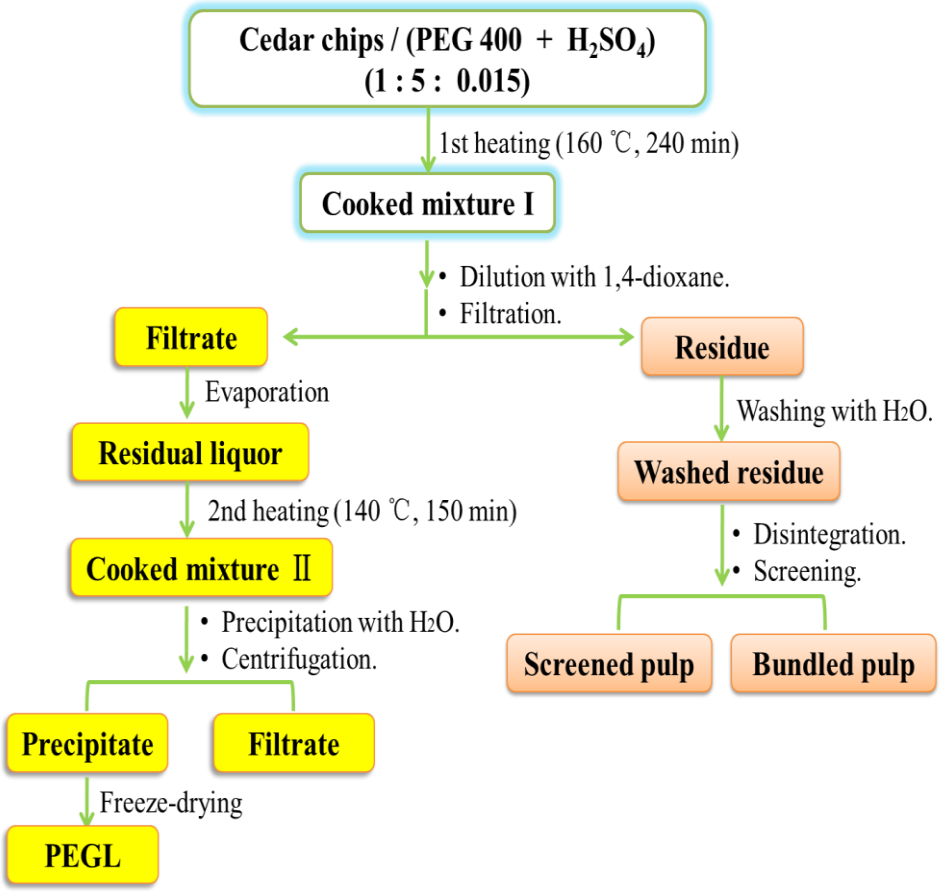

Figure 10. Experimental Scheme for preparation of PEGL

2.2.2 Electrospinning of HAL and its thermostabilization

HAL was dissolved in AcOH or binary solvents of AcOH/CCl_4 (weight ratio, 8:2) at the concentration range of 30-40 wt% with shaking for about 1 h. Different amounts of hexamine (0-10 wt% on solution) were added to the lignin solution, and the mixture was stirred for 2 h at 80 ^{o}C.

An electrospinning machine was manufactured by the Machinery Lab. in Faculty of Science, Hokkaido University, and was composed of a power supplier, a syringe, a nozzle, a drum collector, as shown in **Figure 5**. The syringe with a nozzle of 1.0 mm

diameter was filled with the as-prepared lignin solution, and the electrospinning was conducted under the following conditions: Applied voltage was 38 kV; Positive electrode was connected to the nozzle; Collector was connected to ground; distance between the nozzle and the collector was 13 cm; extrusion rate of solution was about 5 ml h^{-1}. The metallic drum collector was wrapped with a sheet of aluminum foil.

The electrospun HAL fibers were thermostabilized by heating from room temperature to 250 ^{o}C at heating rates of 0.1, 0.3, 0.5, 2 and 3 ^{o}C min^{-1} in air atmosphere, and the temperature was kept for 1 h. This process was carried out in an electronic muffle furnace (KDF S90/S90G, Denken Co. Ltd., Kyoto, Japan).

2.2.3 Electrospinning of PEGL and its thermostabilization

PEGL was dissolved in AcOH/CCl_4 binary solvents (weight ratio, 8:2), at the concentration range of 25-40 wt% with shaking for about 1 h. Hexamine (10 wt%, based on solution) was then added to the lignin solution, and the mixture was stirred for 2 h at 80 ^{o}C.

The syringe with a nozzle of 1.0 mm diameter was also filled with the as-prepared lignin solution, and the electrospinning was carried out under the same conditions as mentioned in HAL fibers preparation: Applied voltage, 38 kV; distance between the nozzle and the collector, 13 cm; extrusion rate of solution, about 5 mL h^{-1}.

The electrospun PEGL fibers were heated from room temperature to 250 ^{o}C at heating rates of 2 ^{o}C/min in air atmosphere, and the temperature was kept for 1 h in

the same electronic muffle furnace.

2.2.4 Electrospinning of SL and its thermostabilization

SL was dissolved in DMF to make solutions with different concentrations (30 and 35 wt. %) and transferred to the syringe. The solutions were subjected to dry electrospinning at room temperature (r.t.) under the following conditions: 25 kV; solution flow rate, 0.05 ml min^{-1}; and tip-collector distance, 13 cm.

In addition, SL with a small amount of PEG 500,000 was also attempted. SL was blended with PEG 500,000 in DMF to make a mixture of 35 wt.%. The weight ratio of SL and PEG 500,000 mixtures was 99/1 or 95/5. The mixture was heated at 80 ℃ for 2.5 h with electromagnetic stirring to make a miscible solution. Then, the solution was subjected to electrospinning in accordance with the aforementioned procedure.

Electrospun SL fibers were thermostabilized in a similar procedure as HAL fibers. The SL fibers were put in a glass plate, and then the plate placed in the muffle furnace. Then, the fibers were heated to 250 ℃ at the rate of 5 ℃ min^{-1} in an air atmosphere and kept at the temperature for 1 h.

2.2.5 Melt spinning of PEGL and its chemical thermostabilization

As shown in **Figure 6**, PEG-lignin was spun by using a laboratory spinning apparatus with a single hole nozzle (diameter: 0.8 mm), manufactured at Mechanical lab, Technical Division, Faculty of Science, Hokkaido University, at the nozzle

temperature of 180 ^{o}C and the winding rates of 45 m min^{-1} under a nitrogen pressure (Uraki et al., 1995; Lin et al., 2012).

The melt spun PEGL fibers were immersed in aqueous HCl solution at concentrations of 6 M at 100 ^{o}C for 2 h. After the chemical treatment, the resultant fibers were washed twice with distilled water, and then roughly dried in an oven at 105 ^{o}C for 2 h (Lin et al., 2012).

2.2.6 Carbonization

All lignin based-fibers were heated from room temperature to 1000 ^{o}C at a heating rate of 3 ^{o}C min^{-1} under a stream of nitrogen (flow rate, 0.5 L min^{-1}) in the furnace, and the temperature was kept for 1 h. After cooling, carbon fibers (CFs) were obtained.

2.2.7 Steam activation

The resultant CFs were heated in the furnace from r.t. to 900 ^{o}C at a heating rate of 10 ^{o}C min^{-1} under a N_2 stream (flow rate, 0.5 L min^{-1}). After reaching the temperature, steam was generated by a heater working at 150 ^{o}C with different amount of H_2O, and mixed with the N_2 gas stream. Such humid N_2 was introduced into the furnace for 1 h. The amount of introduced H_2O was 105 and/or 180 mL.

2.2.8 Characterization

2.2.8.1 Measurement of PEG content

The scheme for measurement of PEG content in PEGL was briefly shown in **Figure 11**. A mixture of 0.2 g PEGL sample and 5 mL hydroiodic acid solution (57 wt.%) was placed in a branched eggplant flask, a N_2 flow was introduced into the flask with a pipette as a flow nozzle. Another eggplant flask containing 25 mL of 20 % potassium iodide solution was set to collect the iodine generated. The mixture was first heated at 145 ^{o}C for 90 min and then, after cooling, all contents in the glass vessels were washed out with 125 mL of 20% potassium iodide solution. After addition of 5 mL of 1% starch solution as an indicator to the solution washed out from the flask, iodometric titration with 0.1 mol/L sodium thiosulfate solution was conducted. Each sample (including the blank) was measured at least twice. The PEG content within PEGL sample was thus expressed as follows,

$$\text{PEG (wt. \%)} = [(V_s - V_b) / 1000] \times 0.1 \times (44 / 2) \times (1 / W_s)$$

where: V_s ——titration volume of $Na_2S_2O_3$ for a sample (mL);

V_b ——titration volume of $Na_2S_2O_3$ for blank (mL);

W_s ——sample weight (g);

0.1——concentration of sodium thiosulfate solution (mol L^{-1});

44 ——formula weight of <EO> (g mol^{-1}).

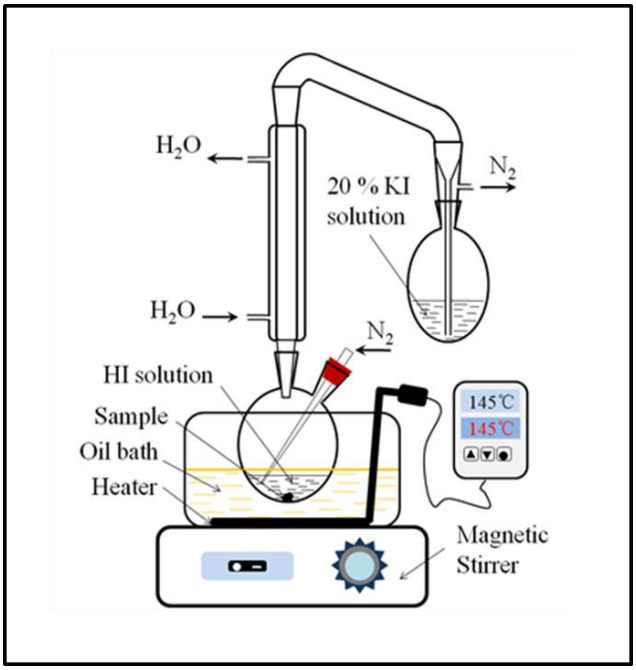

Figure 11. Scheme for PEG content measurement

2.2.8.2 Thermomechanical analysis (TMA)

TMA was conducted on a TMA-4000S System (MAC Science System 010, MAC Science, Yokohama, Japan) under a constant load of 5 g at a temperature range of 30 to 300 ℃ under a N_2 flow of 0.15 L min^{-1}. The glass transition temperature (T_g) and thermal flow-starting temperature (T_f) were estimated from the first and second transition points in the TMA profiles, respectively (Kubo et al. 1996).

2.2.8.3 Images and fiber diameter measurement

Fiber morphology was observed under an optical microscope (Violet laser

color 3D profile microscope VK-9500, Keyence Japan, Osaka, Japan), or on a scanning electron microscope (SEM) (JSM-6301F [FE-SEM], JOEL Ltd., Tokyo, Japan) at an accelerating voltage of 5 kV after gold spattering. Fiber diameters were obtained from the images by averaging the diameters of 20 fibers.

2.2.8.4 Surface area and porosity measurement

N_2 adsorption/desorption of test specimen was measured on a surface area analyzer (Quantachrome, Autosorb-1) at -196 ^{o}C. Prior to the measurement, the specimen was heated at 300 ^{o}C for 3 h at about 10^{-5} Pa. The specific surface area was calculated from N_2 adsorption isotherms in the range of the relative pressure (P/P_0) from 0.02 to 0.30, according to the Brunauer, Emmett, and Teller (BET) model (Fitzer and Müller, 1975). The total pore volume and average pore size were calculated from desorption isotherm, based on Dollimore Heal (DH) model (Kaneko, 1994). In addition, the internal and external surface area can be find out, according to *t*-plot method in the relative pressure range of 0.2～0.5.(Wang et al., 2012)

2.3. Results and discussion

2.3.1 ACFs from electrospun HAL fibers

HAL was dissolved in AcOH to prepare homogeneous solution as a dope at a concentration range of 30-40 wt%. The HAL solution was then subjected to electrospinning. **Figure 12** clearly shows that electrospun fibers was able to be

obtained from the solution at 35 and 40 wt% concentrations at an applied voltage of 38 kV, suggesting that relatively high concentration was required for the spinning. Average diameters of the HAL fibers from 35 wt% and 40 wt% solutions were 1.30 and 1.51 μm, respectively (**Table 1**).

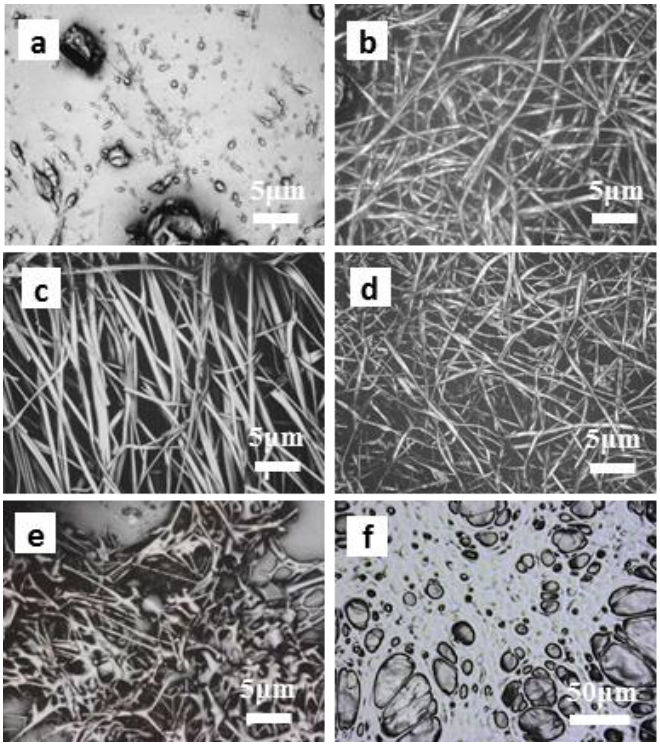

Figure 12. Microscopic images of electrospinning products at different concentrations of HAL/AcOH solution, a), 30 wt%; b), 35 wt%; c), 40 wt%, and thermostabilization products at different heating rates, d), 0.1^{o}C min^{-1} ; e), 0.3^{o}C min^{-1}; f), 0.5^{o}C min^{-1}. (precusor, electrospun fiber derived from 35 wt% HAL/AcOH solution)

Table 1. Electrospinning conditions and average diameters of electrospun fibers

Solution	Solution concentration (%)	Hexamine content (%)	Average diameter (μm)
HAL/AcOH	30	0	-
HAL/AcOH	35	0	1.30
HAL/AcOH	40	0	1.51
HAL/AcOH	35	10	-
HAL/AcOH/CCl_4	35	5	1.51
HAL/AcOH/CCl_4	35	7.5	3.80
HAL/AcOH/CCl_4	35	10	5.17

Since HAL and its fibers have thermal fusibility, the electrospun fibers were subjected to the thermostabilization as a second process for preparation of CFs, in which fusible fibers were converted to infusible ones. In general, it was performed by gradual heating of the fibers to about 250 ^{o}C in an air atmosphere (Kubo et al., 1998). During this process, lignin molecules were oxidized by the oxygen in air and further crosslinked, resulting in the lignin fibers with high thermostability (Faruk and Sain, 2015). Unfortunately, the HAL fibers were melted during the heating even at relatively slow heating rate of 0.3 and 0.5 ^{o}C min^{-1} to lose fibrous morphology. The product morphologies are also shown in **Figures 12d** and **12f**. The thermostabilized fibers could possibly be obtained only at the heating rate of 0.1 ^{o}C min^{-1}. This heating rate meant that it took 38 h for thermostabilization, indicating that this process was

not viable because of dissipation of much time and energy. Accordingly, these electrospun HAL fibers were not suitable as a precursor of CFs, even though such a very slow thermostabilization process could be useful to obtain fine fibers with an average diameter of 0.87 μm.

To accelerate the thermostabilization, one feasible method is to further introduce a crosslinker into lignin molecules. Based on this assumption, hexamine was attempted to be mixed with HAL, because hexamine is decomposed to generate formaldehyde, which acts as a crosslinker for phenol-formaldehyde resin, and ammonia under acidic conditions (Martin et al., 2006). When hexamine was mixed with HAL/AcOH solution, however, the resultant solution was unable to be electrospun. The reason why HAL/AcOH/hexamine solution was not suitable for electrospinning was caused by the high viscosity of the solution: the crosslinking reaction quickly began upon the addition of hexamine in AcOH to increase the solution viscosity.

Hence, HAL and hexamine were dissolved in binary solvents, AcOH/CCl_4, to suppress an increase in solution viscosity, because the viscosity of CCl_4 (0.97 mPa s, 20^{o}C) was smaller than that of AcOH (1.21 mPa s, 20^{o}C), and acidity of the solution was weaker than AcOH alone. Expectedly, HAL was successfully electrospun from such a mixture solution at 35 wt% concentration, as shown in **Figure 13**. **Table 1** summarizes the spinning conditions and the average diameter of the obtained fibers, where missing values in average diameter show unsuccessful electrospinning. The average diameter of electrospun fibers were increased with an increase in hexamine

concentration. These results indicate that a larger amount of hexamine might combine many lignin molecules to give big molecular bundles.

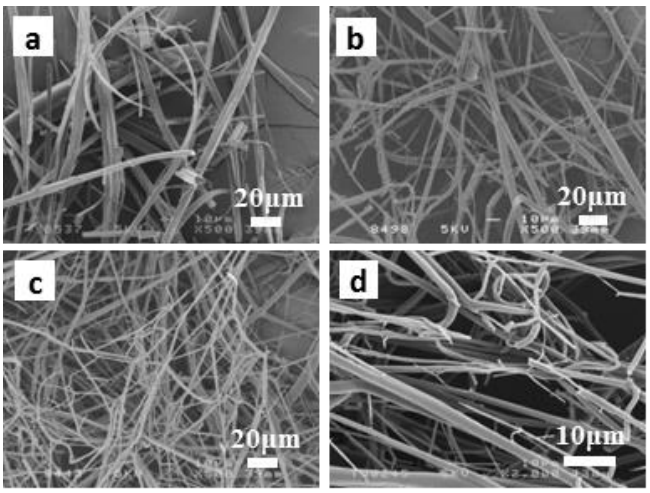

Figure 13. SEM images of lignin based fibrous products at 10 wt% of hexamine content, a), electrospun fibers; b), thermostabilized fibers; c), E-HAL-CF; and d) E-HAL-ACF-105.

As-spun fabrics (fiber mat) containing 7.5 and 10% of hexamine were easily converted to thermostabilized ones by heating in air up to 250^{o}C at a heating rate of 2 ^{o}C min^{-1}, followed by standing at this temperature for 1 h. However, the fabrics with 5% hexamine were partly melted during this process. Thus, thermostabilization time was remarkably shortened from 38 h to less than 3 h by the addition of hexamine, and the average diameter of fibers were also decreased by this thermostabilization from 3.80 to 3.72 μm for the fibers with 7.5 wt% hexamine, from 5.17 to 3.49 μm for those with 10 wt% hexamine as shown in **Table 1** and **2**.

Table 2. Diameter of the resultant fibers after heat treatment

Samples	Hexamine content (%)	Heating rate (^{o}C)	Average diameter (μm)
Thermostabilized fibers	7.5	2	3.72
Thermostabilized fibers	10	2	3.49
E-HAL-CF	7.5	2	2.53
E-HAL-CF	10	2	1.73
E-HAL-ACF-105	10	2	1.42
E-HAL-ACF-180	10	2	1.34

The thermostabilized HAL electrospun fibers with hexamine were converted to CFs by carbonization at 1000 ^{o}C for 1h under a N_2 stream (**Figure 13**). The average diameters of the resultant CFs prepared from the HAL fibers at 7.5 wt% and 10 wt% of hexamine content were 2.53 μm and 1.73 μm, respectively. Therefore, thinner CFs were obtained at 10 wt% of hexamine. Interestingly, the surface of CFs derived from HAL/AcOH solution was very smooth, while the CFs obtained from the mixture solution in binary solvents exhibited a large amount of cracks and pores (**Figure 14**). The mechanism of pore generation is assumed as follows: AcOH is a good solvent for HAL, therefore, strongly interacts with HAL. As a result, unsolvated CCl_4 is easily evaporated from spinning dope to generate the pores during coagulation process of electrospinning, and the porous morphology of the fibers are maintained even after the following heat treatment such as carbonization and steam activation.

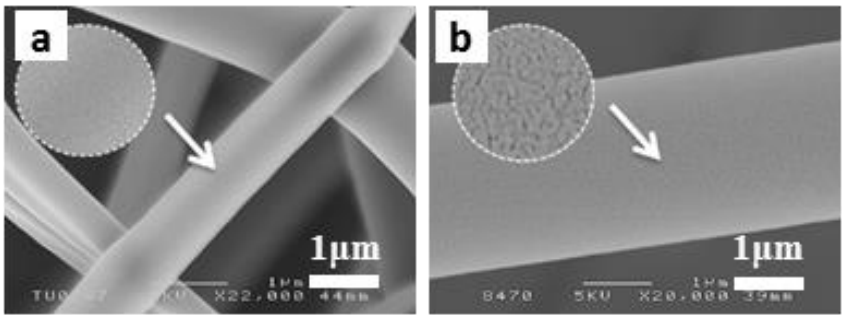

Figure 14. Magnified SEM images of CF derived from a) a single solvent system and b) a binary solvent system (E-HAL-CF)

The CFs (E-HAL-CF) prepared from HAL at 10% of hexamine were, in turn, activated with steam at 900^{o}C for 1 h to prepare ACFs (E-HAL-ACF). The average diameter of E-HAL-ACF-105 (105 mL of H_2O introduced) was 1.42 µm, which was significantly decreased by the carbonization and activation. Additionally, E-HAL-ACF-180 (180 mL of H_2O introduced, SEM images not shown here) was also prepared and it exhibited the similar morphology with an average diameter of 1.34 µm.

2.2.2 ACFs from Electrospun PEGL fibers

PEGL was dissolved in AcOH/CCl_4 binary solvents to prepare homogeneous solutions at the concentration range of 25-40 wt% and subjected to electrospinning. **Figure 15** clearly shows that electrospun fibers were obtained from the solution concentration of 30-40% at an applied voltage of 38 kV. Diameters of the PEGL fibers from 30 to 40 wt% solutions were in the range from 2.11 to 3.32 µm (**Table 3**),

and the solution with a lower concentration gave thinner fibers. However, all the fibers were melted during thermostabilization at a heating rate of 2 ^{o}C min^{-1}, which was similar as untreated electrospun HAL fibers (You et al., 2015b).

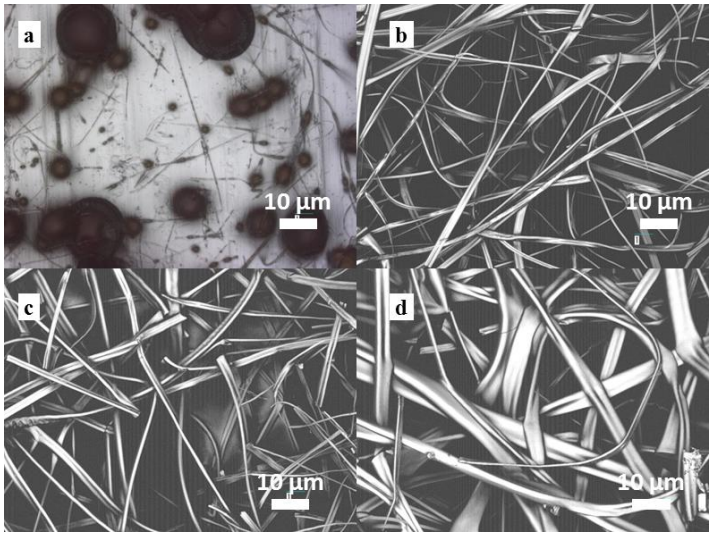

Figure 15. Microscopic images of electrospinning products with different HAL/AcOH/CCl_4 solution concentration, a), 25wt %; b), 30 wt%; c),35 wt%; d),40 wt%.

Table 3 Electrospinning condition and average diameter of electrospun fibers

	solution	**Solution concentration (%)**	**Hexamine content (%)**	**Average diameter (µm)**
1	PEGL/AcOH/CCl_4	25	0	-
2	PEGL/AcOH/CCl_4	30	0	2.11
3	PEGL/AcOH/CCl_4	35	0	3.32
4	PEGL/AcOH/CCl_4	40	0	5.16
5	PEGL/AcOH/CCl_4	30	10	4.42

In the previous section, hexamine was introduced to HAL solution system to increase the thermostability of HAL fibers. Accordingly, I also attempted to add 10% of hexamine to PEGL/AcOH/CCl_4 solution in this fiber preparation. As shown in **Figure 16a**, fine fibers (4.42 μm in diameter) can be obtained. **Figure 16b** shows that PEGL fibers could be thermostabilized by a heating rate of 2℃ min^{-1} for a conventional oxidative treatment with air.

After carbonization and activation, the average fiber diameters of the ACFs activated with 105 mL of water (E-PEGL-ACF-105) and the ACFs activated with 180 mL of water (E-PEGL-ACF-180) decreased from 2.93 μm to 1.57 and 1.23 μm, respectively (**Table 4**).

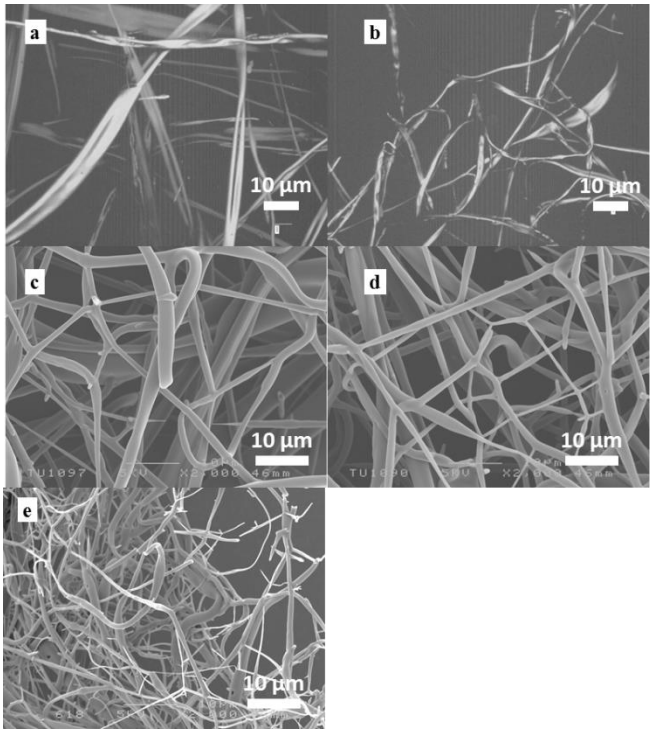

Figure 16. SEM images of PEGL based fibrous products with 10 wt% hexamine a) electrospun fibers; b) thermostabilized fibers c) CFs; d) E-PEGL-ACF-105; e) E-PEGL-ACF-180

Table 4. Diameters of fibers after heat treatment

	Samples	Hexamine content (%)	Average diameter (μm)
1	Thermostabilized fibers	10	2.93
2	E-PEGL-CFs	10	2.06
3	E-PEGL-ACF-105	10	1.57
4	E-PEGL-ACF-180	10	1.23

2.3.3 ACFs from electrospun SL fibers

Electrospinning of SL alone in DMF was found to be impossible. The addition of PEG was reported to improve spinnability of lignin (Dallmeyer et al., 2010). Therefore, I tried to improve the spinnability of SL with PEG. By using PEG 500,000, fine fibers were obtained. Here, the procedure was briefly explained. SL was mixed with PEG 500,000 with a ratio of 99/1 in DMF (35 wt. %) in a heating bath (80 ℃). The heated mixture was subjected to electrospinning at applied of voltage 24~26 kV. As a result, thin fibers with an average diameter of 0.85 μm were obtained (**Figure 17a**). However, when the content of PEG 500,000 increased, the solution could not be spun constantly.

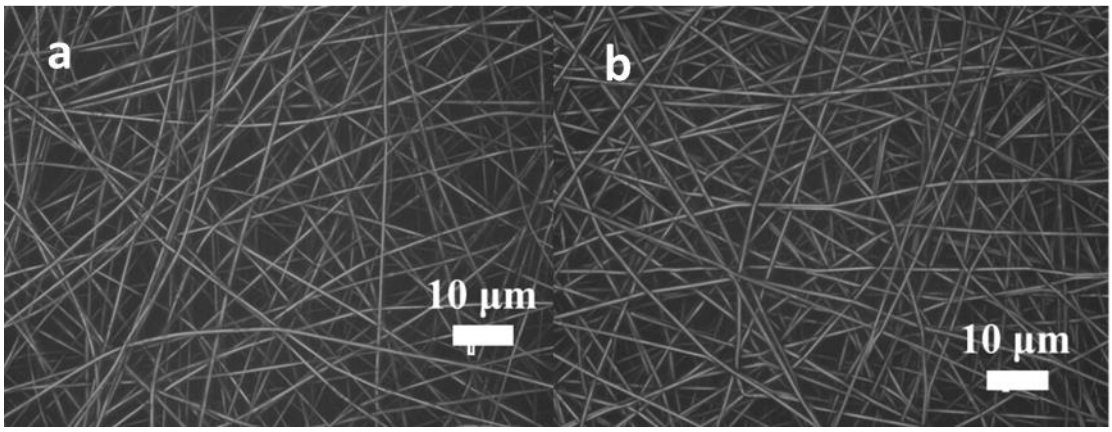

Figure 17. Microscopic images of electrospun SL fibers a) before thermostabilization; b) after thermostabilization at 5 ^{o}C min^{-1}

As for SL fibers, it was found that the normal oxidative thermostabilization with air was enough to obtain thermostabilized fibers. The maximum heating rate was 5 ℃ min^{-1}. As shown in **Figure 17b**, the thermostabilized SL fibers maintained fiber morphology.

The CFs derived from SL electrospun fibers (E-SL-CF) with a diameter of 0.7 μm were obtained at a yield of 34 % on thermostabilized fibers, as shown in **Figure 18a**. Interestingly, E-SL-CF showed many distinctive pores on the surface, indicating SL fibers were easily burned off during carbonization.

Surface area and pore volume of carbonaceous materials can be further developed by steam activation. E-SL-CF was heated from room temperature at 10 ^{o}C min^{-1} to 900 ^{o}C, under a N_2 stream of 0.5 L min^{-1}. When furnace temperature reached 900 ^{o}C, water was dropped onto the hot plate to generate steam, and the steam was introduced with a N_2 flow for 1 h. For SL fibers, 180 mL water flow was used for the

activation, and the obtained fiber was referred to E-SL-ACF-180 (**Figure 18b**).

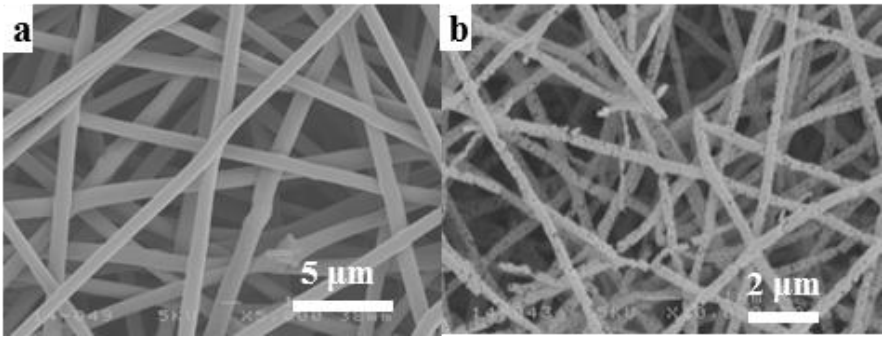

Figure 18. SEM image of (a) E-SL-CF and (b)E-SL-ACF-180

E-SL-ACF-180 was obtained at a yield of 70 % (based on E-SL-CF). **Figure 18b** showed the morphology of SL-ACF-180. Compared with PEGL-ACFs and HAL-ACFs, SL-ACF-180 showed a pretty smaller fiber diameter of 270 nm, and a more porous structure on the surface and inside of fibers.

2.3.4 ACFs from melt spun PEGL fibers

A PEGL with a PEG content of 46.4% was obtained by organosolv pulping. The T_g and T_f of this PEGL were determined by TMA to evaluate the thermal properties. As shown in **Figure 19**, the TMA profile of PEGL displays two transition points at 106.6 ℃ and 173.5 ℃, which correspond to the T_g and T_f, respectively (Kubo et al. 1996). These two transition temperatures are slightly lower than those of hardwood AAL, which has a T_g of 128 ℃ and a T_f of 177 ℃ (Uraki et al. 1995). Therefore, fusible PEGL is more thermally active than AAL. PEGL may be a more suitable material for melt spinning.

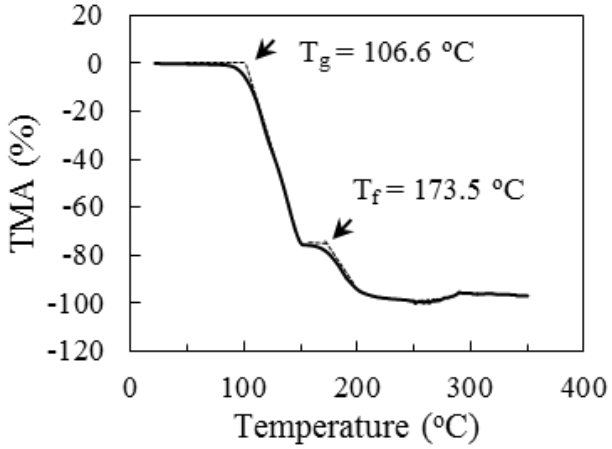

Figure 19. TMA of PEGL powder

The SEM images in **Figure 20** clearly show the changes in fiber morphology after the conversion process of the melt-spun fibers to ACFs. The melt-spun PEGL fibers showed an average diameter of 37.7 μm and a smooth surface. With the chemical thermostabilization, cracks were generated in the fibers. After carbonization and activation, the average fiber diameters of the ACFs activated with 105 mL of water (M-PEGL-ACF-105) and the ACFs activated with 180 mL of water (M-PEGL-ACF-180) decreased to 23.1 and 20.6 μm, respectively. Comparing the surface morphology of both ACFs, M-PEGL-ACF-180 appears to be more porous than M-PEGL-ACF-105.

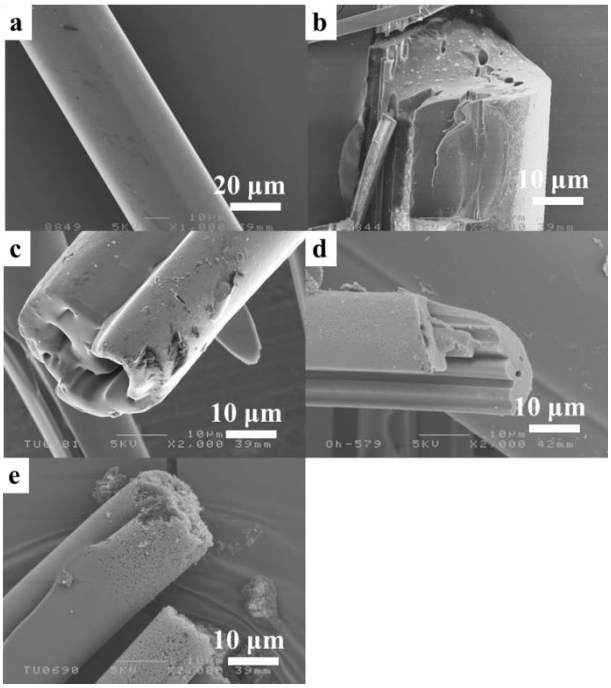

Figure 20. SEM images of PEGL based fibrous products: (a) melt-spun fibers; (b) chemical thermostabilized fibers; (c) carbon fibers; (d) M-PEGL-ACF-105; and (e) M-PEGL-ACF-180.

2.2.5 Surface area and pore size distribution

Table 5 shows the BET surface area and average pore size of all carbonaceous samples, and AC powder was used as a reference. M-PEGL-CF and E-HAL-CF had large BET surface areas of 1338 and 1287 m^2 g^{-1}, respectively, which were almost comparable to that of commercial AC powder (1434 m^2 g^{-1}) in spite of not being activated. Such large surface area of thick M-PEGL-CF may be attributed to the cracked surface morphology generated by the chemical thermostabilization process (Lin et al. 2012), and the large surface area of E-HAL-CF was contributed by the pores generated from using binary solvents in electrospinning process. E-PEGL-CF had a closed surface area of 1136 m^2 g^{-1}, whereas E-SL-CFs had a smaller value of

635 m^2 g^{-1}.

All CFs were converted to ACFs under the same activation conditions with 105 and/or 180 mL of H_2O introduction at 1000 ℃. As shown in **Table 5**, large amount of H_2O used in activation results in large surface area in each series of ACF samples. The BET surface area of the M-PEGL-ACF-180 and E-HAL-ACF-180 was largely increased to 2460 and 2447 m^2 g^{-1} with average diameters of 1.7 and 1.8 nm, respectively. The surface area of the E-PEGL-ACF-180 was a little smaller (2095 m^2 g^{-1}) with similar average pore diameter of 1.8 nm. When 105 mL of H_2O was introduced, only E-HAL-ACF-105 showed a surface area (2185 m^2 g^{-1}) larger than 2000 m^2 g^{-1} among all ACFs samples, and a small average diameter of 0.9 nm. In contrast, the BET surface area of the E-SL-ACF-180 was only 1411 m^2 g^{-1}. In addition, its average pore diameter of 4.73 nm was much larger than that of other ACFs.

The internal surface area, as a measure of micro- and mesoporous volumes, was calculated by the *t*-plot method. The external surface areas of both M-PEGL-ACF-180 and E-PEGL-ACF-180 were in a similar range around 700-800 m^2 g^{-1}. In contrast, the internal surface area showed a large value larger than 1200 m^2 g^{-1}, suggesting that the ACFs mainly consist of micro- and mesopores. More specifically, the internal surface area of M-PEGL-ACF-180 was nearly 1.5 times higher than that of E-PEGL-ACF-180.

In addition, E-HAL-ACF-180 showed a similar value of internal surface area (1278 m^2 g^{-1}) to that of external surface area (1169 m^2 g^{-1}) and that of AC powder,

suggesting nearly equivalent pores size distribution between micro/meso- and macropores in E-HAL-ACF-180. Compared with E-HAL-ACF-180, the less activated sample E-HAL-ACF-105 exhibit a much larger internal surface area of 1775 m^2 g^{-1} and a smaller external surface area of 410 m^2 g^{-1}, indicating abundant micro-/mesospores were existed. Specifically, the pores of E-HAL-ACF-105 is rich in the range of 0.5-1.3 nm, while that of E-HAL-ACF-180 is converted to a larger region of 1.3-3.0 nm as shown in **Figure 21**. On the other hand, the AC powder had a large value of external surface area revealed that most pores consisted of macropores that do not involve in adsorption of guest molecules (**Table 5**). This difference in pore size distribution among E-HAL-ACF-105, E-HAL-ACF-180 and AC powder might affect the accumulation of the electrolyte ions, when EDLC is assembled with these materials.

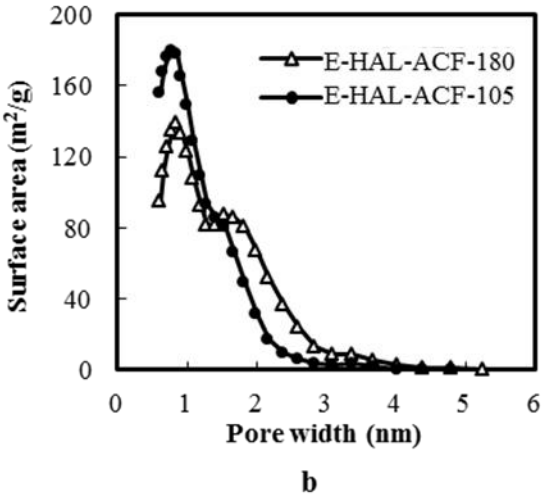

Figure 21. Surface area distribution of carbon materials in the pore range of 0.6-5.0 nm (calculated by using a slit pore QSDFT model)

In contrast, E-SL-ACF-108 showed the lowest surface area of 1411 m^2 g^{-1} with the largest average pore diameter of 4.7 nm, even though it is thinnest fibers among all samples.

It has been reported that the difference in the BET surface area and the pore size distribution affects the electric performance of the EDLCs (Chmiola et al. 2006). Therefore, I proceeded EDLCs assembly by using all kinds of ACFs as electrode materials.

Table 5. Surface area and pore diameters of carbonaceous materials

Samples	S_{BET} (m^2 g^{-1}) [a]	DFT ave pore diameter (nm) [b]	Internal surface area (m^2 g^{-1}) [c]	External surface area (m^2 g^{-1}) [c]
AC powder	1434	1.5	331	1103
E-HAL-CF	1287	0.9	1158	129
E-HAL-ACF-105	2185	0.9	1775	410
E-HAL-ACF-180	2447	1.8	1278	1169
E-PEGL-CF	1136	0.8	1039	97
E-PEGL-ACF-105	1443	0.9	1308	135
E-PEGL-ACF-180	2095	1.8	1288	807
E-SL-CF	635	3.0	567	67
E-SL-ACF-180	1411	4.7	922	489
M-PEGL-CF	1338	1.1	1256	81
M-PEGL-ACF-105	1649	0.9	1498	151
M-PEGL-ACF-180	2461	1.7	1745	716

[a] Calculated by the BET model.

[b] Calculated based on the QSDFT model.

[c] Calculated according to the *t*-plot method.

Chapter 3 Single cell type electric double layer capacitors (SC-EDLCs) assembly and their electrochemical performance by using different electrolytes

3.1 Introduction

Electric energy storage in EDLCs is caused by the formation of electric double layer on the surface of both electrodes. The surface area of the electrodes is a crucial factor to increase electrostatic capacitance. Therefore, ACFs with large surface area are used as a main electrode constituent (Pandolfo and Hollenkamp, 2006; Simon and Burke, 2008). On the other hand, the species of the electrolyte solutions is another important factor that affects the EDLC capacitance, which is resulted from the different efficiency of ion adsorption/desorption on/from carbonaceous constituent (Inagaki et al., 2010).

I selected the ACFs preparations with large surface area derived different lignins as an electrode constituent. Basically, ACFs (E-HAL-ACF-105/180, E-PEGL-ACF-180 and M-PEGL-ACF-180) prepared in the previous chapter with surface area large than 2000 $m^2 g^{-1}$ were used to prepare electrodes for SC-EDLC in this chapter. E-SL-ACF-180 was also used for SC-EDLC assembly, although the surface area was only 1411 $m^2 g^{-1}$. Commercial AC powder was used for comparison.

In addition, both organic and aqueous electrolyte solutions were used to explore the optimum electrolyte systems for each ACFs sample.

3.2 Experimental

3.2.1 Materials

Aluminum foil (0.1 mm in thickness, 99.99% of purity) and Nickel foam were purchased from The Nilaco Corporation (Tokyo, Japan) and Sumitomo Electric Industries, Ltd. (Osaka, Japan), respectively. Conductive carbon black (CB, Super P conductive, 99+ %) were purchased from Alfa Aesar (Heysham, UK). Propylene carbonate (PC, Battery Grade), Potassium hydroxide (KOH), carboxymethyl cellulose sodium salt (CMC) and commercial activated charcoal (AC) were purchased from Wako Pure Chemical Industries, Co., Ltd. in Japan. Triethylmethylammonium tetrafluoroborate ($TEMABF_4$) was purchased from Tokyo Chemical Industry Co., Ltd. Polytetrafluoroethylene (PTFE, 60 wt % dispersion in H_2O) was purchased from Sigma-Aldrich Co. LLC. in Japan. All chemicals were used as received without further purification. Paper (Type-A sheet) as a separator was kindly supplied from Mitsubishi paper Mills Ltd. Tokyo, Japan. Polyethylene (PE) separator was purchased from Nippon Sheet Glass Co. Ltd. Tokyo, Japan.

3.2.2 Electrolyte preparation

Two different kinds of electrolyte solutions were prepared in this study. Herein, 1.0 M $TEAMBF_4$/PC solution was used as organic electrolyte solution, and 6.0 M KOH aqueous solution were used as aqueous electrolyte solutions.

3.2.2 Electrodes preparation

3.2.2.1 Al Electrodes for organic electrolyte

Carbonaceous samples, such as AC powder and ACFs, were ground with a pestle and a mortar. This ground sample was added to 2 wt% of aqueous CMC solution (weight ratio of sample to CMC, 85 : 10) , and then the mixture was ultrasonicated for 2 h by using an ultrasonicator (5510R-DTH, Branson Ultrasonics, Emerson Japan Ltd.) to give homogeneous slurry. Separately, CB was added to the suspension of carbonaceous sample and CMC (sample:CMC:CB = 85:10:5). A few droplets of theses suspensions were dropped onto Al foil, and the droplets were spread by rolling a steel stick to form a thin layer. After drying in an oven at 105 ^{o}C overnight, the coated Al foil was cut into circle form (diameter, 16 mm). This Al foil was kept in oven at 105 ^{o}C before EDLC assembly. The solid weight on the Al foil was calculated by the difference in weight between before and after deposition of samples. These sample-coated Al foils were used as an electrode for SC-EDLCs with organic electrolyte.

3.2.2.2 Ni Electrodes for aqueous electrolyte

The electrode for SC-EDLCs with an aqueous electrolyte was composed of carbonaceous samples (AC powder, ACFs), CB, and PTFE. The weight ratio of carbonaceous samples/CB/PTFE was 85/5/10. The carbonaceous samples and CB were first mixed and ground until the mixture was homogenized. The mixture was

then blended with 6 wt% PTFE/water emulsion as a binder, and homogenized by using a pestle and a mortar. Subsequently, ethanol was added in the mixture for PTFE demulsification, and the softened paste-like mixture was repeatedly rolled into sheets with approximately 100 μm thickness by using a steel stick. The resultant sample sheets were then put on the Ni foam (used as a current collector) and followed by repeated rolling to connect the coated sample and Ni foam matrix were tightly. Finally, the sample coated Ni foam was cut into 16 mm diameter circle sheet and further dried at 105 ℃ overnight to obtain Ni-electrodes.

3.2.3 SC-EDLC assembly

Figure 22 shows vertical cross section of SC-EDLC. Two sheets of current collectors deposited with carbonaceous samples (loading weight, 1-3 mg for Al-electrodes; 10-30 mg for Ni-electrodes) were used as electrodes for SC-EDLC assembly. In one SC-ELDC, the total weight of electrode constituents between upper and lower sheets was kept almost identical (weight difference of two sheets, 0.1 mg for Al-electrodes; 1 mg for Ni-electrodes).

In the case of organic electrolyte system, the Al-electrodes and a piece of paper sheet (2 cm in diameter, 33 μm in thickness) as a separator were immersed in organic electrolyte solution (1.0 M $TEAMBF_4$/PC solution), and the foil and the sheet was degassed *in vacuo* for 3h at room temperature.

Similarly, the Ni-electrodes and a piece of PE separator were used in aqueous electrolyte system. All electrodes and the separator were immersed in 6.0 M KOH

aqueous solution, and degased under the same condition as mentioned above.

The SC-EDLCs assembly processes are the same for both organic and aqueous electrolyte systems. One electrode was placed on the bottom of flat cell device (Eager Corporation, Japan), and one separator was put on the foil. Afterwards, another electrode was placed on the separator like as sandwich. Finally, steel plate, which was connected to an analyzer, was placed on the upper Al foil.

All the processes for EDLC assembly were carried out under N_2 atmosphere with a very low humidity (RH< 5%) in a glove box.

3.2.4 Characterization

3.2.4.1 Electrochemical property

The performance of the prepared SC-EDLC was evaluated by cyclic voltammetry (CV), electrochemical impedance spectroscopy (EIS), and galvanostatic charge/discharge (GCD) method using an electrochemical workstation (Autolab PGSTAT302N FRA32M, Metrohm Autolab B.V., Japan).

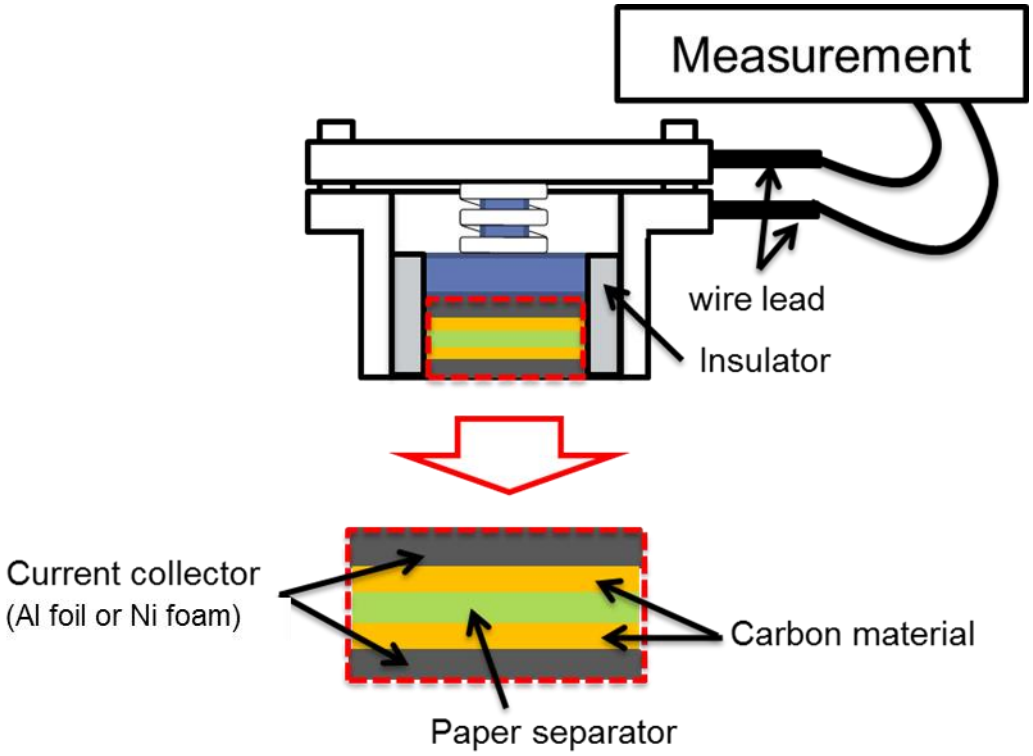

Figure 22. Structure of SC-EDLC

Cyclic voltammgram curves were monitored at different scan rate within a potential window of 0-3.0 V for organic electrolyte system. In the case of aqueous electrolyte system, CV profiles were obtained in the potential window of 0-1.0 V at the scan rate of 0.005 V s^{-1}. The specific capacitance was calculated according to the following formula(Davies and Yu, 2011):

$$C_{\text{device}} = \frac{\int i dt}{m \cdot \Delta V} \qquad (1)$$

Where i (A) is the current detected by the electrochemical workstation; t is time (s) of charge or discharge process; ΔV (V) is the scanning potential range; and m (g) stands for the total weight of the electrode constituents on two electrodes. Because the area integration in equation (1) is difficult to calculate, equation (1) was simplified as the following equation:

$$C_{\text{device}} = \frac{I}{m \cdot V/t} \qquad (2)$$

Where I (A) is the current formed at the potential of 1.5 V for organic electrolyte system, and 0.5 V for aqueous electrolyte system (intermediate value in the potential range), V/t (V s^{-1}) is the potential scanning rate and m (g) stands for the total weight of the materials on two electrodes.

Due to electrodes with almost the same weight of electrode materials were selected to assemble the EDLC, which can be treated as symmetric electrodes, so the specific capacitance of single electrode could be calculated according to the following formula:(Qu and Shi, 1998)

$$C_{\text{electrode}} = 4\, C_{\text{device}} \qquad (3)$$

GCD measurements were carried out at current density of 1 A g^{-1} within the voltage range of 0-3 V for organic electrolyte system and 0.05 A g^{-1} at 0-1 V for aqueous electrolyte system. The specific capacitance of each device was calculated from the GCD curves using the formula:

$$C_{\text{device}} = \frac{i}{m \cdot dV/dt} \qquad (4)$$

Where i is the current applied (in amps, A), dV/dt is the slope of the discharge curve (in volts per second, V s^{-1}), and m refers to the total weight (in gram, g) of the materials on two electrodes including carbon materials, CMC, and CB. The $C_{\text{electrode}}$ can be calculated by equation (4).

It is worth mentioning that all the values of specific capacitance in the following parts are used $C_{\text{electrode}}$ for description.

EIS experiments were carried out at open circuit potential with a sinusoidal signal with amplitude of 10 mV over a frequency range of 100 kHz to 1 Hz.

The impedance of EDLC is caused by charge transfer, electrolyte ions diffusion and etc., which can be simulated as an equivalent circuit (named as Randles equivalent circuit) in **Figure 23**. In the circuit, C_{dl} is double layer capacitance and W is Warburg impedance, which is caused by electrolyte ions diffusion.

The Nyquist Plot (one of EIS) for this circuit is shown in **Figure 24** and the ideal charge transfer resistance can be calculated according to the following equation:

$$(Z_{Re} - R_e - \frac{R_{ct}}{2})^2 + {Z_{Im}}^2 = (\frac{R_{ct}}{2})^2 \qquad (5)$$

where Z_{Im} is impedance in imaginary part and Z_{Re} is impedance in real part. R_e is the equivalent series resistance, and it is also defined as intrinsic resistance in some references (Wang et al., 2001; Liu et al., 2008). It should be mentioned that the Nyquist plot of real EDLC is complex, so charge transfer resistance is described as the chord length of the simulated impedance circle (equation (5) means a circle in mathematics), which is semi-quantitative.

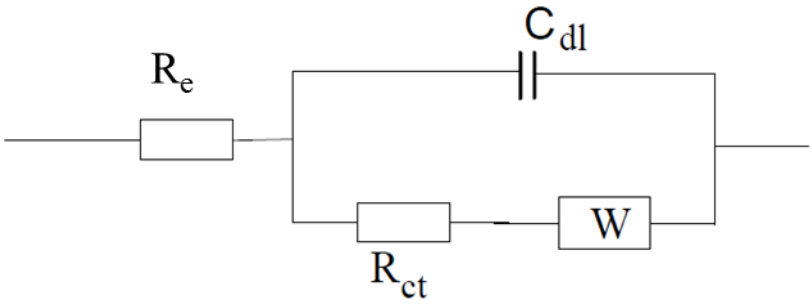

Figure 23 Randles equivalent circuit

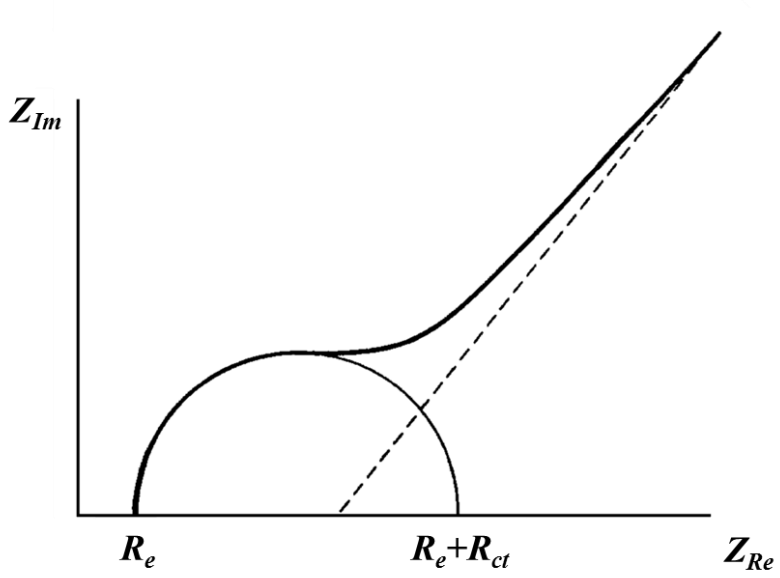

Figure 24 Nyquist diagram for randles equivalent circuit

3.3 Results and discussion

3.3.1 Electrochemical properties of SC-EDLCs with organic electrolyte

3.3.1.1 E-HAL-ACFs as electrode materials

The electrodes of the EDLC were fabricated with ground E-HAL-ACF-105 and E-HAL-ACF-180 as a main electrolyte-holding material together with CB as a conductive material and CMC as a binder. The EDLC was assembled with such electrodes and an organic electrolyte ($TEMABF_4$/PC). These constituents for EDLC were assembled in a pair of electrodes as a symmetrical cell. The electrochemical property of the resultant EDLCs were evaluated by using cyclic voltammetry (CV), galvanostatic charge/discharge (GCD) method, and electrochemical impedance spectroscopy (EIS). The data or profiles are shown in **Figures 25** to **27**, respectively.

All CV profiles were monitored at a potential window from 0 to 3 V at different scan rates of 0.01, 0.05, and 0.1 V s^{-1}. The cyclic voltammogram of $EDLC_{E\text{-}HAL\text{-}ACF\text{-}105}$ show a nearly rectangular shape, indicating that the electric double layer was well formed. The calculated values of electrostatic capacitance were from 135 F g^{-1} at the scan rate of 0.1 V s^{-1} to 143 F g^{-1} at the scan rate of 0.01 V s^{-1}, as shown in **Figure 25a**. These results indicate that the EDLC has a good capacitive behavior and high-scan-rate stability. On the other hand, the EDLC assembled with AC powder showed a lower value of 74.8 F g^{-1}at a scan rate of 0.05 V s^{-1}(**Figure 25b**). Even though the E-HAL-ACF-180 had a larger surface area

than E-HAL-ACF-105, which might provide more adsorption sites for electrolyte ions and result in large electrostatic capacitance, it only showed a low capacitance of 69.2 F g^{-1}. This huge difference was because E-HAL-ACF-105 had more abundant pores distributed in 0.5-1.3 nm than E-HAL-ACF-180 as shown in chapter 2, which was identified with the finding that pores less than 1 nm lead to a significant increase in carbon capacitance (Chmiola et al., 2006). Because the solvated electrolyte ions become highly distorted when they squeeze through such small pores, and such distortion would allow closer approach of the ion center to the electrode surface, which leads to improved capacitance.

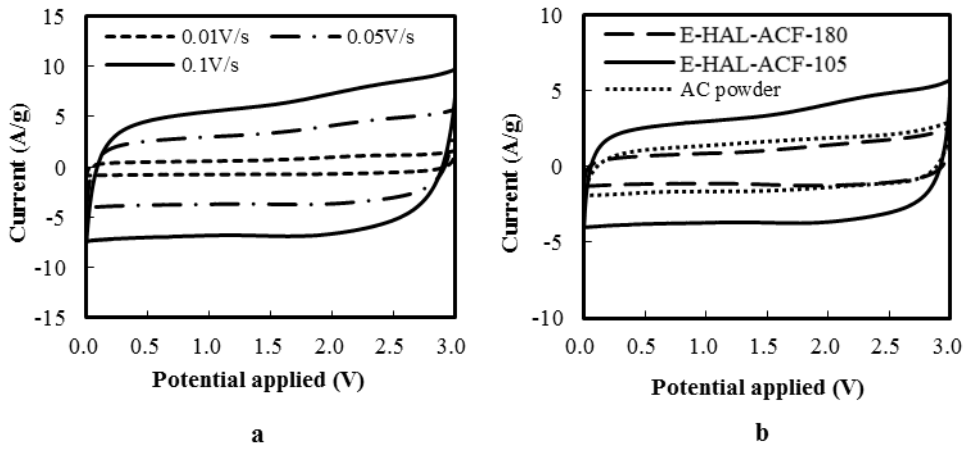

Figure 25. Cyclic voltammograms of $EDLC_{E\text{-}HAL\text{-}ACFs}$ and $EDLC_{AC\ powder}$. a) $EDLC_{E\text{-}HAL\text{-}ACF\text{-}105}$ at different scan rates and b) comparison of $EDLC_{E\text{-}HAL\text{-}ACF\text{-}180}$, $EDLC_{E\text{-}HAL\text{-}ACF\text{-}105}$ and $EDLC_{AC\ powder}$ at 0.05 V s^{-1}.

In GCD measurements, the profile of $EDLC_{E\text{-}HAL\text{-}ACF\text{-}105}$ and $EDLC_{E\text{-}HAL\text{-}ACF\text{-}180}$ showed symmetrical triangles, and this triangle shape was repeatedly shown until 100 times even at a high current density of 1 A g^{-1} (**Figure 26a and b**). These results also indicated the effective formation of electric-double-layer. The specific capacitance of

$EDLC_{E\text{-}HAL\text{-}ACF\text{-}105}$ from GCD was calculated as 133.3 F g^{-1} **(Figure 26a)**, which was superior to $EDLC_{E\text{-}HAL\text{-}ACF\text{-}180}$ (63.5 F g^{-1}, **Figure 26b**) and AC powder (65.2 F g^{-1}, **Figure 26c**). It was also comparable to those assembled with other different ACFs, which were prepared from commercial synthetic polymers (Inagaki et al., 2010). The high performance of $EDLC_{E\text{-}HAL\text{-}ACF\text{-}105}$ was attributed to the large surface area and proper pore size distribution.

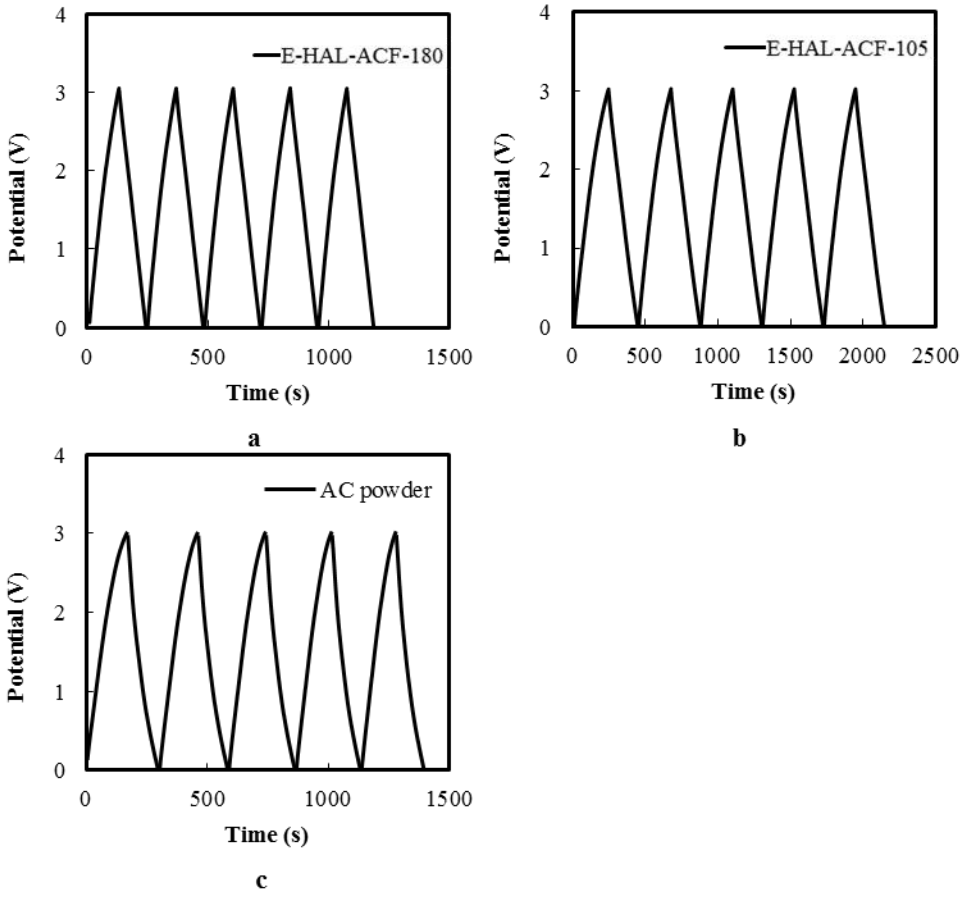

Figure 26. GCD profiles of a) $EDLC_{E\text{-}HAL\text{-}ACF\text{-}180}$, b) $EDLC_{E\text{-}HAL\text{-}ACF\text{-}105}$ and c) $EDLC_{AC\ powder}$ under a current density of 1 A g^{-1}

Figure 27 shows Nyquist plots of EDLCs assembled with E-HAL-ACFs and AC powder in a frequency range from 100 kHz to 1 Hz. Both profiles show one semicircle at

the high-frequency region (low Z' area) and slope line at the low-frequency region (high Z' area). The intrinsic resistance is obtained at the intercept on the *Z'* axis in Nyquist plots at the high-frequency region, and the intrinsic resistance is the sum of the resistances of the electrolyte and the ACFs and of the contact resistance between the ACFs and the current collector (Liu et al. 2008; Liu et al. 2012). Both $EDLC_{E\text{-}HAL\text{-}ACF\text{-}105}$ and $EDLC_{E\text{-}HAL\text{-}ACF\text{-}180}$ show lower intrinsic resistance of 1.1 Ω than that of AC powder (2.4 Ω) at the intercept of Z' axis (Liu et al., 2008; Lu et al., 2012).

A charge transfer resistance, as a measure of electrolyte mobility for adsorption and desorption rates of the electrolyte onto/from the pores of carbonaceous consitituent, can be obtained from the diameter of the semicircle at the high-frequency region (Liu et al., 2008). The charge transfer resistance of $EDLC_{E\text{-}HAL\text{-}ACF\text{-}105}$ (12.0 Ω) was larger than those of $EDLC_{E\text{-}HAL\text{-}ACF\text{-}180}$ (3.1 Ω) and $EDLC_{AC\ powder}$ (3.1 Ω), suggesting that the adsorption and desorption rates of the electrolyte onto/from E-HAL-ACF-105 were slower than those onto/from E-HAL-ACF-180 and AC powder. In addition, the line length of slope at the angle of 45^{o} in low frequency region means diffusion resistance in the pore (**Figure 28**) (Liu et al., 2008). The length in the profile of $EDLC_{E\text{-}HAL\text{-}ACF\text{-}105}$ was also longer than that of $EDLC_{E\text{-}HAL\text{-}ACF\text{-}180}$ and $EDLC_{AC\ powder}$, indicating E-HAL-ACF-105 electrode has a high diffusion resistance. The insufficient mobility of the electrolyte is probably caused by the smaller pore size distribution of E-HAL-ACF-105 (0.5-1.3 nm) than those of E-HAL-ACF-180 (1.3-3.0 nm) and AC powder (macropores).

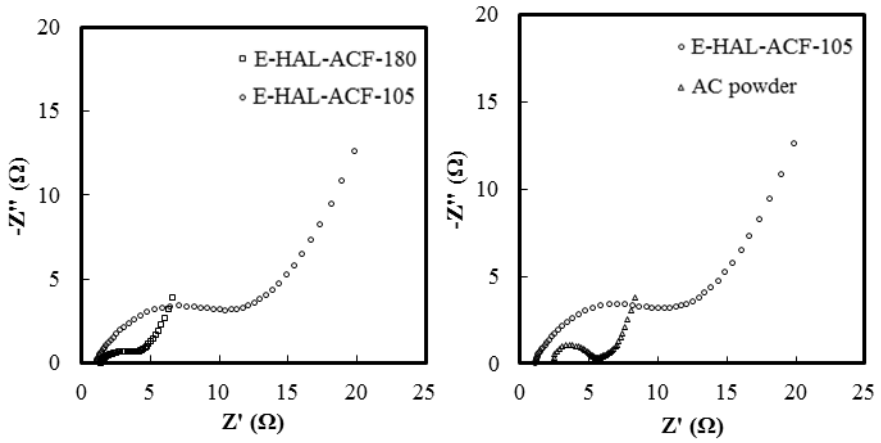

Figure 27. Nyquist plots of E-HAL-ACF-180, E-HAL-ACF-105 and AC powder based EDLCs

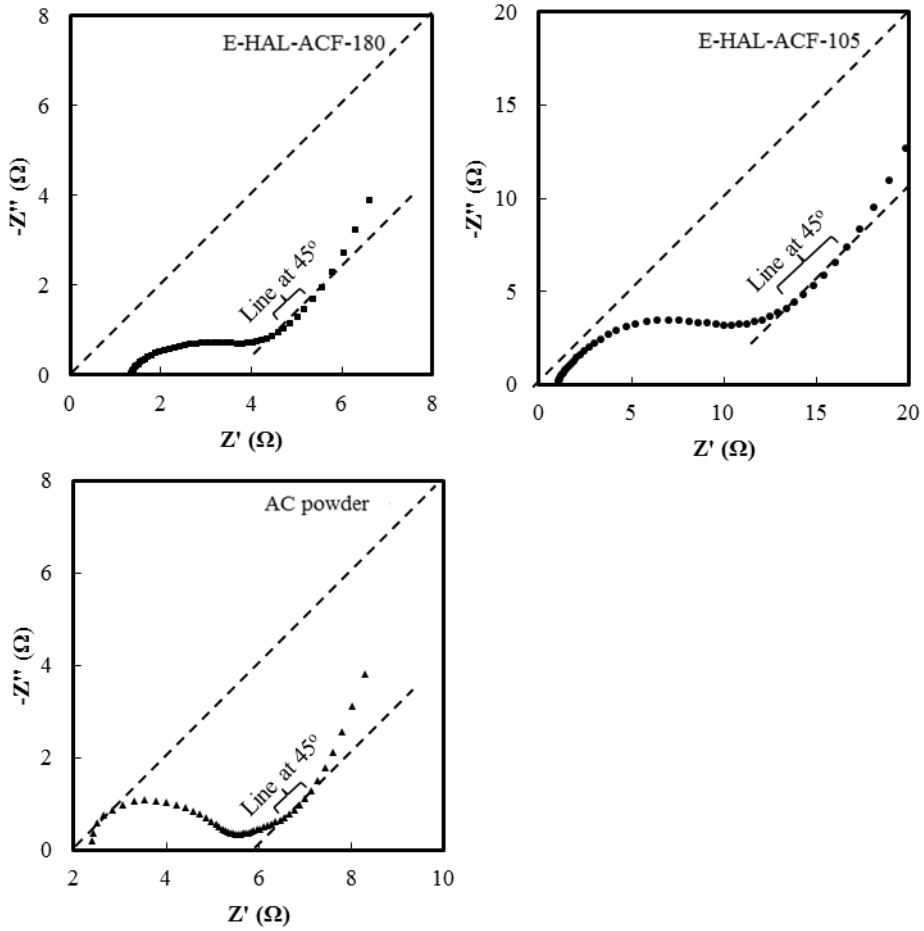

Figure 28. Diffusion resistance of E-HAL-ACFs and AC powder represented in the Nyquist plots.

3.3.1.2 E-PEGL-ACF-180 as electrode materials

The electrochemical performance of $EDLC_{E\text{-}PEGL\text{-}ACF\text{-}180}$ was summarized in **Figure 29**. Typical rectangular CV curves of $EDLC_{E\text{-}PEGL\text{-}ACF\text{-}180}$ with 1 M $TEMABF_4$/PC organic electrolyte were obtained at the scan rate of 0.05 V s^{-1} with the potential window of 0-3 V. From CV profile, a specific capacitance was estimated to be 44.7 F g^{-1}.

The GCD method was also adopted to measure the capacitance of EDLCs. The charge/discharge profile of $EDLC_{E\text{-}PEGL\text{-}ACF\text{-}180}$ was obtained at a constant current density of 1 A g^{-1} with the potential window of 0-3 V. The charge/discharge curves of $EDLC_{E\text{-}PEGL\text{-}ACF\text{-}180}$ were approximately symmetric and linear, suggesting good electrochemical stability and reversibility. Based on GCD profiles, the specific capacitance of $EDLC_{E\text{-}PEGL\text{-}ACF\text{-}180}$ was calculated to be 54.9 F g^{-1}, which is a little lower than that of $EDLC_{E\text{-}HAL\text{-}ACF\text{-}180}$ (63.5 F g^{-1}). It was because E-PEGL-ACF-180 possessed a smaller surface area (2095 m^2 g^{-1}) than E-HAL-ACF-180 (2447 m^2 g^{-1})

Nyquist plots of $EDLC_{E\text{-}PEGL\text{-}ACF\text{-}180}$ showed a depressed semi-circle at high frequency and straight lines at low frequency. The profile also indicated the intrinsic resistance and charge transfer resistance were 1.6 Ω and 0.6 Ω, respectively. These results showed that $EDLC_{E\text{-}PEGL\text{-}ACF\text{-}180}$ had almost the same intrinsic resistance as that of $EDLC_{E\text{-}HAL\text{-}ACF\text{-}180}$ (1.1 Ω) and a lower charge transfer resistance than that of $EDLC_{E\text{-}HAL\text{-}ACF\text{-}180}$ (2.4 Ω), suggesting the penetration rate of the organic electrolyte on E-PEGL-ACF-180 were faster than those on E-HAL-ACF-180.

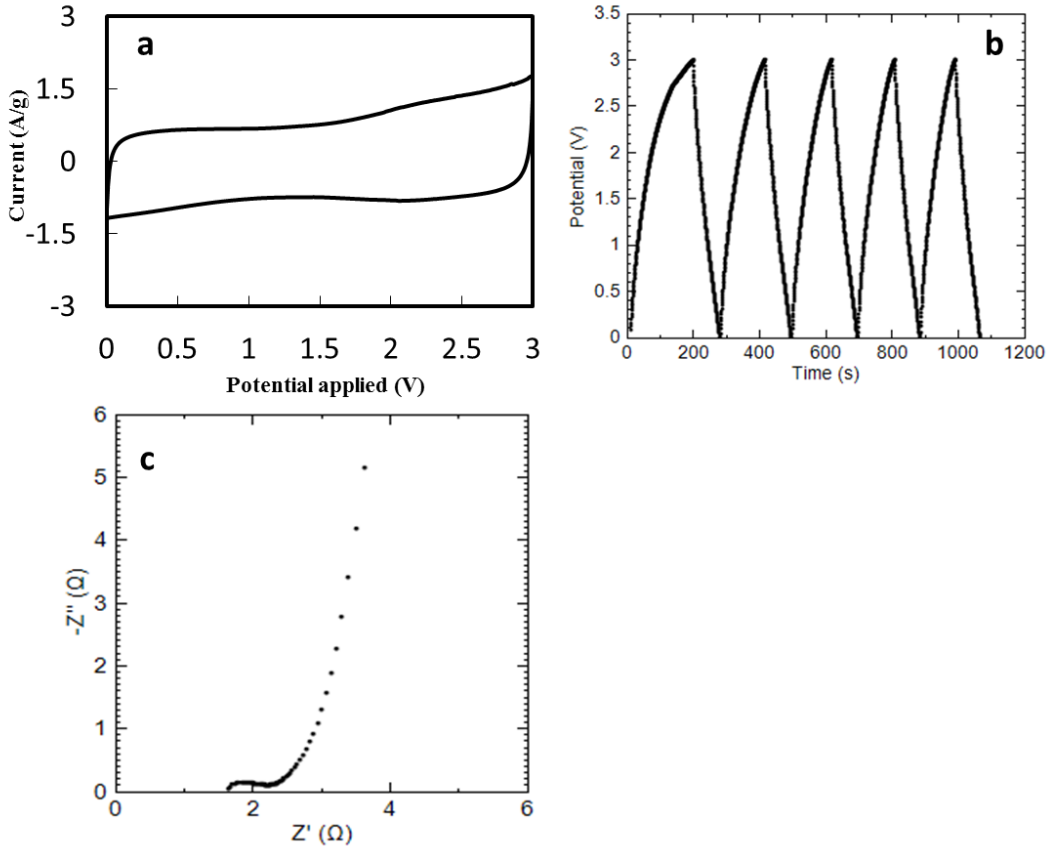

Figure 29. Electrochemical characterizaiton of $EDLC_{E\text{-}PEGL\text{-}ACF\text{-}180.}$ a) Cyclic voltammogram, b) GCD profile, and c) Nyquist plot.

3.3.1.3 E-SL-ACF-180 as electrode materials

The electrochemical performance of and $EDLC_{E\text{-}SL\text{-}ACF\text{-}180}$ was also evaluated by CV, GCD and EIS. CV measurements were conducted at three different scanning rates of 0.01, 0.05 and 0.1 V s^{-1} between 0 and 3.0 V. The obtained CV curves are shown in **Figure 30a**. All the CV curves of $EDLC_{E\text{-}SL\text{-}ACF180}$ obtained at all scan rates showed the typical rectangular shape, suggesting the adequate formation of an electric double layer. At scan rates of 0.01, 0.05 and 0.1 V s^{-1}, the specific capacitances were calculated to be 57.5, 53.2 and 54.2 F g^{-1}, respectively.

Figure 30b shows GCD profile of $EDLC_{E\text{-}SL\text{-}ACF\text{-}180}$ at a current density of 1 A g^{-1}. $EDLC_{E\text{-}SL\text{-}ACF\text{-}180}$ exhibited a slightly asymmetrical triangular shape, indicating a relatively low charge–discharge efficiency compared with EDLC prepared from HAL and PEGL electrospun fibers mentioned before. Accordingly, $EDLC_{E\text{-}SL\text{-}ACF\text{-}180}$ had a small specific capacitance of 55.6 F g^{-1} at 1 A g^{-1}.

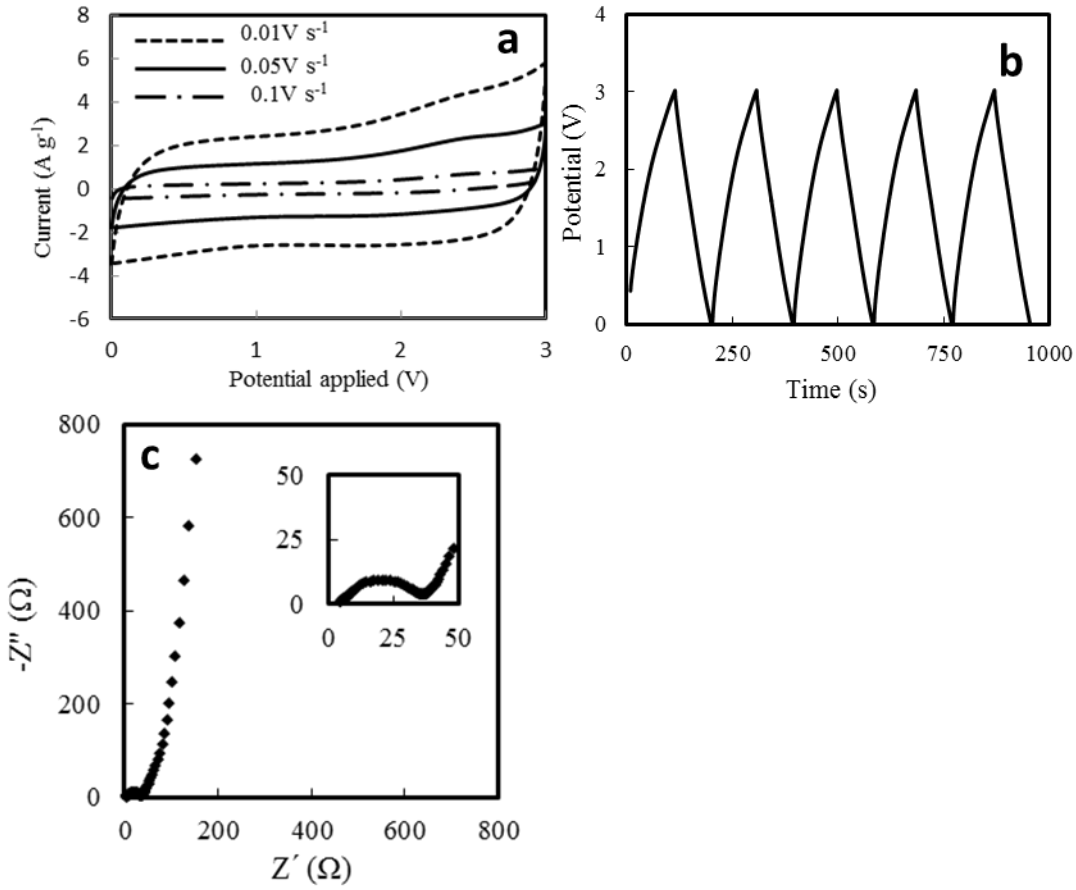

Figure 30. Electrochemical characterizaiton of $EDLC_{E\text{-}PEGL\text{-}ACF\text{-}180.}$ a) Cyclic voltammograms at different scan rates, b) GCD profile, and c) Nyquist plot (The inset is a magnification of the high-frequency region).

According to the Nyquist plot (**Figure 30c**), $EDLC_{E\text{-}SL\text{-}ACF\text{-}180}$ possess an intrinsic

resistance of 4.5 Ω and a large charge transfer resistance of 33.5 Ω (**Table 6**). This inferior performance of $EDLC_{E\text{-}SL\text{-}ACF\text{-}180}$ was attributed to the smaller BET surface area (1411 m^2 g^{-1}) and the larger pore size of SL-ACFs compared with those of other ACFs preparations (Chmiola et al. 2006). A carbonaceous material with a larger surface area can contain more electrolyte ions. In addition, the adsorption of electrolyte ions on the smaller pores of the material facilitates the contact between the ions and the material. As a result, carbonaceous materials with large surface areas and small pore diameters give a large capacitance to EDLC.

Table 6 Electrochemical performances of SC-EDLCs

Samples	1M $TEMABF_4$/PC			6M KOH		
	Capacitance ($F\ g^{-1}$)	Intrinsic resistance (Ω)	Charge transfer resistance (Ω)	Capacitance ($F\ g^{-1}$)	Intrinsic resistance (Ω)	Charge transfer resistance (Ω)
E-HAL-ACF-105	133.3	1.1	12.0	—	—	—
E-HAL-ACF-180	63.5	1.1	3.1	—	—	—
E-PEGL-ACF-180	54.9	1.6	0.6	121.2	0.7	1.5
E-SL-ACF-180	55.6	4.5	33.5	—	—	—
M-PEGL-ACF-180	109.5	2.3	3.2	84.2	0.6	1.1
AC powder	65.2	2.4	3.1	140.2	1.5	—

3.3.1.4 M-PEGL-ACF-180 as electrode materials

As shown in **Figure 31**, the CV curves of SC-EDLC prepared with M-PEGL-ACF-180 was almost rectangular shaped in the applied potential range of 0-3 V at a scan rate of 0.05 V s^{-1}, suggesting good capacitive behavior. The same profile was obtained until 5 CV cycles, which indicated that the electrolyte was not decomposed in the potential window.

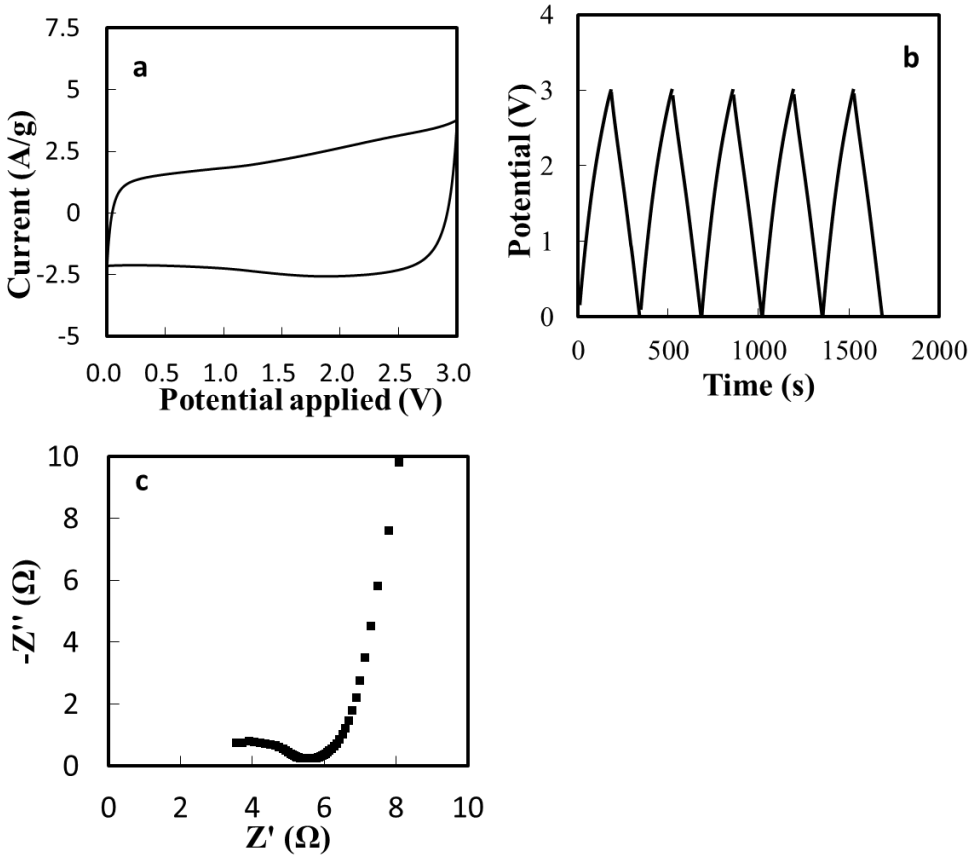

Figure 31. Electrochemical properties of $EDLC_{M\text{-}PEGL\text{-}ACF\text{-}180}$: (a) CV curves at a scan rate of 0.05 V s^{-1}; (b) GCD profiles, and (c) the Nyquist plot.

The electrostatic capacitance was calculated from the area of the CV curves. Although the profiles are a deformed rectangle, the area was calculated based on an approximate

rectangle, where the long side of the rectangle was the potential window and the short side was the current difference between the upper and lower lines at an applied potential of 1.5 V. Similarly, the specific capacitance was also calculated from the tangent of the GCD curves in the discharging process (**Figure 31b** and **31c)**. The GCD profile for $EDLC_{M\text{-}PEGL\text{-}ACF\text{-}180}$ was monitored at a current density of 1 A g^{-1}. As summarized in Table 6, the specific capacitance of $EDLC_{M\text{-}PEGL\text{-}ACF\text{-}180}$ (109.5 F g^{-1}) was larger than that of $EDLC_{AC\ powder}$ (65.2 F g^{-1}). The superior performance of $EDLC_{M\text{-}PEGL\text{-}ACF\text{-}180}$ should be attributed to the large surface area of M-ACF-180 (2461 m^2 g^{-1}).

The EIS measurement of $EDLC_{M\text{-}PEGL\text{-}ACF\text{-}180}$ showed a similar value of intrinsic resistance and charge transfer resistance as those of $EDLC_{AC\ powder}$ (**Table 6**). This result implied that an adequate electrode conductivity and a sufficient penetration rate of the electrolyte ions into the pores of electrode materials in $EDLC_{M\text{-}PEGL\text{-}ACF\text{-}180}$.

3.3.2 Electrochemical properties of SC-EDLCs with aqueous electrolyte

To investigate the electrochemical performance of SC-EDLC in aqueous electrolyte system, M-PEGL-ACF-180, E-PEGL-ACF-180 and commercial AC powder were used as an electrode constituent to assemble SC-EDLC with 6 M KOH aqueous solution. Due to instability of Al foil and CMC in the strong alkali electrolyte, the Al current collector and binder (CMC) used in organic electrolyte was changed to Ni foam and PTFE, respectively.

The electrochemical performances of SC-EDLC with aqueous electrolyte were also evaluated by CV, GCD and EIS. Due to the electrolysis (decomposition) of water occurring

at a standard potential of -1.23 V (Wikipedia contributors, 2016a), therefore, the scan range in CV measurement was limited in 0-1 V, and the scan rate was set at 0.005 V s^{-1}. The obtained CV curves are shown in **Figure 32**. According to equations (2) and (3) in section 3.2.4.1, the specific capacitances of $EDLC_{M\text{-}PEGL\text{-}ACF\text{-}180}$, $EDLC_{E\text{-}PEGL\text{-}ACF\text{-}180}$ and $EDLC_{AC\ powder}$ were calculated to be 93.1, 44.7 and 103.5 F g^{-1}, respectively.

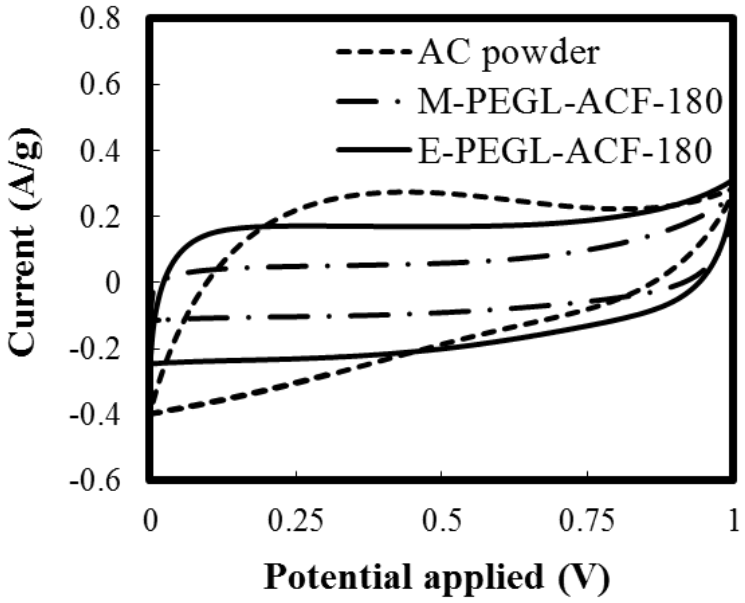

Figure 32. Cyclic voltammograms of $EDLC_{E\text{-}PEGL\text{-}ACF\text{-}180,}$ $EDLC_{M\text{-}PEGL\text{-}ACF\text{-}180}$ and $EDLC_{AC\ powder}$ with aqueous electrolyte at the scan rate of 0.005 V s^{-1}.

Figure 33 shows GCD profiles of $EDLC_{M\text{-}PEGL\text{-}ACF\text{-}180}$, $EDLC_{E\text{-}PEGL\text{-}ACF\text{-}180}$ and $EDLC_{AC\ powder}$ at a current density of 0.05 A g^{-1}. All the EDLCs exhibited the isosceles triangular shapes of the profiles, indicating good charge/discharge performances. However, compared with $EDLC_{AC\ powder}$, both of the $EDLC_{M\text{-}PEGL\text{-}ACF\text{-}180}$ and $EDLC_{E\text{-}PEGL\text{-}ACF\text{-}180}$ showed shorter discharge time, indicating lower capacitances for the $EDLC_{PEGL\text{-}ACFs}$ (**Figure 33a**). In

addition, both $EDLC_{AC\ powder}$ and $EDLC_{E\text{-}PEGL\text{-}ACF\text{-}180}$ with aqueous electrolyte exhibited much larger capacitance than those assembled with organic electrolyte (**Table 6**). These results might be caused by their different pore size distribution: KOH ions were easier to accumulate in large pores, such as large mesopores and macropores, than in small pores, such as micropores and small mesopores. These large pores and small pores are indicated by indicated by external surface area and internal surface area, respectively (Endo et al., 2001). According to the surface area data, large pores were richer in AC powder than in M-PEGL-ACF-180 and E-PEGL-ACF-180. Additionally, the ion size of KOH (cation, 0.36 nm; anion, 0.53 nm) was smaller than that of $TEAMBF_4$ (cation, 0.65 nm; anion, 0.46 nm) (Inagaki et al., 2010). As a result, a larger amount of KOH ions could be accumulated in carbonaceous samples than that of $TEAMBF_4$ ions. Accordingly, ACFs were interior to AC powder as electrode materials assembled with aqueous electrolyte solution.

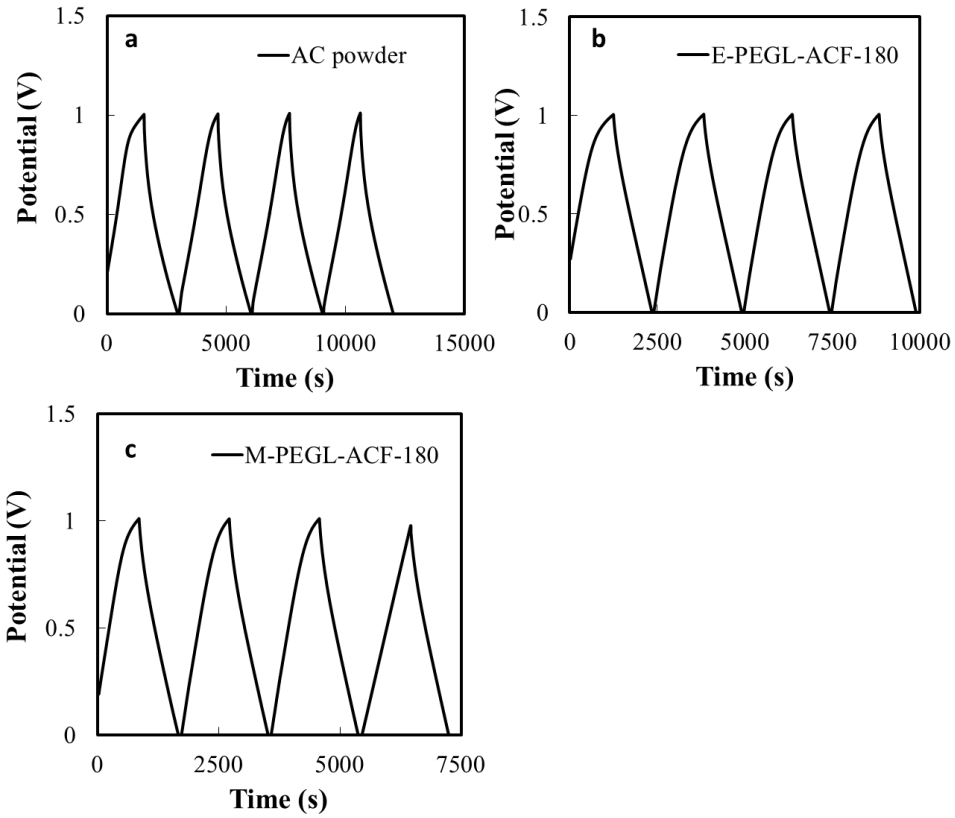

Figure 33. GCD profiles of a) $EDLC_{AC\ powder}$, b) $EDLC_{E\text{-}PEGL\text{-}ACF\text{-}180}$ and c) $EDLC_{M\text{-}PEGL\text{-}ACF\text{-}180}$ under a current density of 0.05 A g^{-1}

The Nyquist plots of $EDLC_{M\text{-}PEGL\text{-}ACF\text{-}180}$, $EDLC_{E\text{-}PEGL\text{-}ACF\text{-}180}$ and $EDLC_{AC\ powder}$ are shown in **Figure 34**. $EDLC_{M\text{-}PEGL\text{-}ACF\text{-}180}$ and $EDLC_{E\text{-}PEGL\text{-}ACF\text{-}180}$ possess lower intrinsic resistances (0.6 Ω and 0.7 Ω, respectively) than $EDLC_{AC\ powder}$ (1.5 Ω), indicating M-PEGL-ACF-180 and E-PEGL-ACF-180 have higher conductivity than AC powder has. In addition, the charge transfer resistances of $EDLC_{M\text{-}PEGL\text{-}ACF\text{-}180}$ and $EDLC_{E\text{-}PEGL\text{-}ACF\text{-}180}$ were 1.1 and 1.5 Ω, respectively. Unlike ACF-based EDLCs, $EDLC_{AC\ powder}$ did not exhibit an arc in the high frequency range but a mild slope in the low frequency range. This result suggested an easy penetration of KOH ions into the pores of AC powder, but the diffusion of KOH ions in AC powder were slower than that in ACFs samples. It is because the physical adsorption

of KOH ions on ACFs directly occurs on the surface but not inside the fibers, where equilibrium concentration of KOH was easily achieved around the ACFs surface; whereas KOH ions first diffused into commercial AC through the macropores, and then penetrated into the micropores, where a concentration gradient of KOH ions might exist from the outside area of the AC powder to the inside area of macropores. Similar adsorption mechanism had also been reported previously (Uraki et al. 1997).

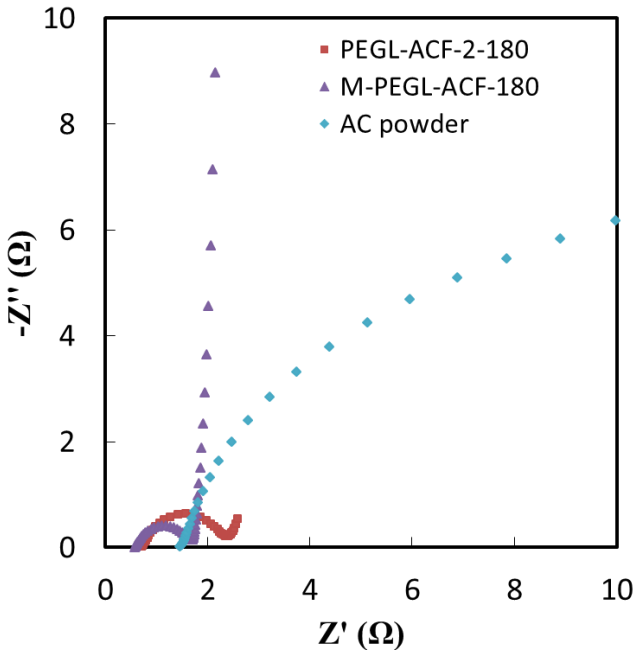

Figure 34. Nyquist plots of $EDLC_{E\text{-}PEGL\text{-}ACF\text{-}180,}$ $EDLC_{M\text{-}PEGL\text{-}ACF\text{-}180}$ and $EDLC_{AC\ powder}$

Chapter 4 Internal tandem electric double layer capacitors (IT-EDLCs) assembly and characterization of their electrochemical performance

4.1 Introduction

It is a main subject to achieve wide operating voltage and high energy density for practical use of EDLCs. However, the operating voltage of SC-EDLC is typically from 1.0 to 3.5 V, which is limited by electrolyte species. Additionally, the energy density of carbon-electrode based SC-EDLC is largely restrained by the ion adsorption capability of carbon electrode, resulting in relatively low energy density of 5 to10 Wh kg^{-1} (Chen et al., 2015). Devices with several SC-ELDCs externally connected in series manner can achieve higher voltages, but this would lead to unavoidable energy losses, due to the increase in system resistances and packing weight (Zhang et al., 2014; Chen et al., 2015).

To overcome this problem, one simple method is to assemble IT-EDLCs, which laminate more than 2 pairs of electrodes in one package and internally connect each pair of electrodes. Although this approach is commonly used in fuel cells (Hu et al., 2006; Rajalakshmi et al., 2008; Lin et al., 2009), it has been studied only in a very few cases of all-solid-state symmetric EDLCs, aqueous electrolyte EDLCs, and organic electrolyte EDLCs (Zhang et al., 2014).

In this chapter, I select M-PEGL-ACF-180 as an example to illustrate the IT-EDLC assembly and its electrochemical property.

4.2 Experimental

4.2.1 Materials

Aluminum foil (0.1 mm in thickness, 99.99%) was purchased from The Nilaco Corporation (Tokyo, Japan). Conductive carbon black (CB, Super P conductive, 99+ %) were purchased from Alfa Aesar (Heysham, UK). Propylene carbonate (PC, Battery Grade), carboxymethyl cellulose sodium salt (CMC) and commercial activated charcoal (AC) were purchased from Wako Pure Chemical Industries, Co., Ltd. in Japan. Triethylmethylammonium tetrafluoroborate ($TEMABF_4$) was purchased from Tokyo Chemical Industry Co., Ltd. All chemicals were used as received without further purification. Paper (Type-A sheet) as a separator was kindly supplied from Mitsubishi paper Mills Ltd. Tokyo, Japan.

4.1.2 Electrode preparation

The ACFs were ground with a domestic mixer, and they were suspended in an 2 wt% aqueous CMC solution together with CB. As a reference, AC powder was used instead of ACFs. The final weight ratio of carbonaceous materials, CMC, and CB was 85:10:5. The suspension was coated on an Al foil with a doctor blade (gap thickness, 100 μm; Eager Corporation, Japan), and the foil was dried in an oven at 105 ℃ to give a single-side coated Al foil. Backside of the single-side coated Al foil was coated again with the above mentioned suspension in the same manner. After drying, a double-side coated Al foil was obtained.

The single-side and double-side coated Al foils were cut into a circular shape and a square shape, which had a rectangular tail at an end for the connection to each other, as shown in **Figure 35b**. The mass of the pieces was measured to calculate the loading weight of solid materials in the suspension on the Al foil. The pieces with a similar weight (weight difference, <0.1 mg) were selected and immersed in the electrolyte solution 1 M $TEMABF_4$/PC to yield electrodes bearing an electrolyte. Similarly, cellulosic paper was also cut into either a circular or square shape and immersed in the electrolyte solution to give a separator.

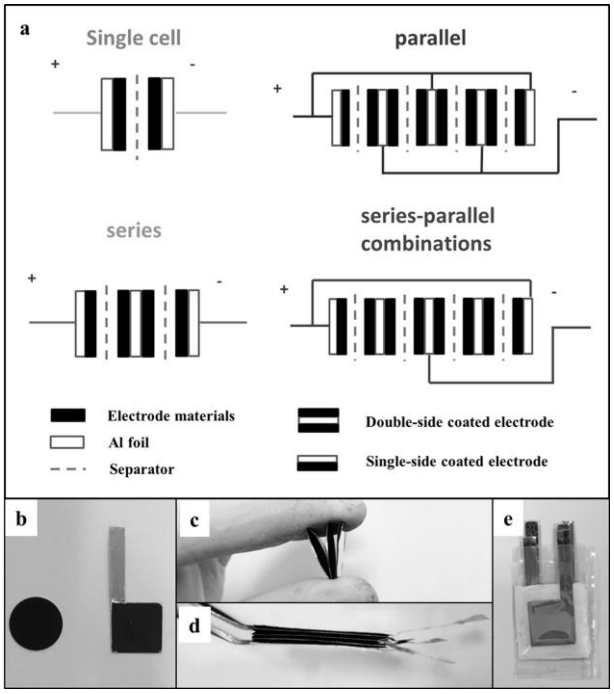

Figure 35. Images of electrodes and their connections. (a) Design images of electrode connection patterns; (b) photo of electrodes with circular and square shapes; (c) photo of electrodes connected in series; (d) photo of electrodes connected in parallel or S/P comb.; and (e) photo of sealed electrodes connected in parallel or S/P comb.

4.1.3 IT-EDLC assembly

To assemble an IT-EDLC, circular-shaped electrodes were connected in series, whereas the square-shaped electrodes were used in IT-EDLCs connected in parallel and in an S/P comb. In the case of the series type, the circular-shaped electrodes were taken out of the electrolyte solution and gently wiped with a cheese cloth to remove the excess solution. According to **Figure 35a**, two single-side electrodes and one double-side coated electrode were laminated together with the separators. Finally, the laminated electrodes were put inside of the measurement cell, and it was sealed in the same way as the SC-EDLC assembly.

Figure 35d and 35e show photos of the parallel and S/P combination connections. Two single-side coated electrodes and three double-side coated electrodes with a square shape were also laminated, where the tail part of each electrode was placed alternatively on the left and right position after they were taken out from the electrolyte solution and wiped. Then, the set of laminated electrodes with separators was put in a plastic bag and sealed by a vacuum sealer so that the tail part was exposed to the outside of the bag. Finally, the tail parts were bound with clips to achieve the above connections.

4.1.4 Characterization

The specific capacitance and impedance of the EDLCs were evaluated using an electrochemical workstation (Autolab PGSTAT302N FRA32M, Metrohm Autolab B.V., Tokyo, Japan). The specific capacitances were measured separately by cyclic voltammetry (CV) and galvanostatic charge/discharge (GCD). CV monitored a potential window of 0-3 V

for parallel-connected IT-EDLC and 0-6 V for IT-EDLCs with series and S/P comb. connections at a scan rate of 0.05 V s^{-1}. GCD was measured at a current density of 1 or 2 A g^{-1}. The specific capacitance was calculated from the cyclic voltammogram and GCD profile, according to equations (2), (3) and (4) in Chapter 3 (Qu and Shi, 1998; You et al., 2015a; You et al., 2015b).

The impedance was measured by electrochemical impedance spectroscopy (EIS) between 100,000 Hz and 0.01 Hz at an AC amplitude of 10 mV, and the intrinsic resistance and polarization resistance were calculated from the EIS Nyquist plots (Liu et al., 2008).

The energy density (*E*) based on the weight of the electrode materials was estimated according to equation (6) (Kim et al., 2013), where the electrode constituents were the carbonaceous material, CB and CMC (except for the Al foil that served as a current collector).

$$E = \frac{1}{8} C V_{max}^2 \qquad (6)$$

where *C* is the specific capacitance calculated from the GCD measurement, and V_{max} is the maximum value of the operating potential window.

The power density (*P*) based on the weight of the electrode materials was obtained from the following equation (Tian et al., 2015):

$$P = \frac{E}{t} \qquad (7)$$

where *t* is the discharge time.

The packaged energy density and power density were calculated based on the following assumptions according to the previous report (Gogotsi and Simon, 2011): the weight ratio of electrode constituents (ACFs, CMC and CB) in a SC-EDLC was estimated to be ca. 30% of

the entire EDLC device, which contained electrode constituents, Al foils, electrolyte, separator and outer package. The percentages of electrolyte and other parts (Al foils, separator, and packing material) were estimated to be 60% and 10%, respectively. Based on this assumption, in the case of the IT-EDLC with the series connection (2 pairs of electrodes), the weight ratio of the electrode material mass/electrolyte/other parts was 40/40/20 (Zhang et al., 2014). Therefore, the packaged energy density and power density were 40% of calculated *E* and *P* values based on electrode constituents.

In the case of the parallel and S/P comb. connections (4 pairs of electrodes), the weight ratio of the electrode material mass/electrolyte/other parts was estimated to be 52/26/22. Similarly, the packaged energy density and power density were 52% of calculated *E* and *P* values based on electrode constituents.

4.3 Results and discussion

4.3.1 IT-EDLC in series connection

The series connected IT-EDLC was fabricated using four pairs of electrodes, corresponding to four SC-EDLCs, in addition to two pairs of electrodes. Its precise CV measurement could not be performed because its potential window was out of the range of our analyzer. Thus, only the IT-EDLC with the series connection of two pairs of electrodes is discussed here. **Figure 36** shows CV curves for a potential window of 0-6 V, and the same curves were obtained by 5 cycles. Thus, the potential window was expanded by the series connection. Similarly, the same profiles of GCD in the range of 0-6 V were obtained until 20 cycles. These data also indicate the stability of IT-EDLCs. In addition, IT-EDLC$_{\text{M-PEGL-ACF-180}}$

exhibited a higher specific capacitance of 82.0 F g^{-1} than IT-EDLC$_{AC\ powder}$ (52.0 F g^{-1}). This result is probably because the larger BET surface area of M-PEGL-ACF-180 gave a larger capacitance to the corresponding EDLC.

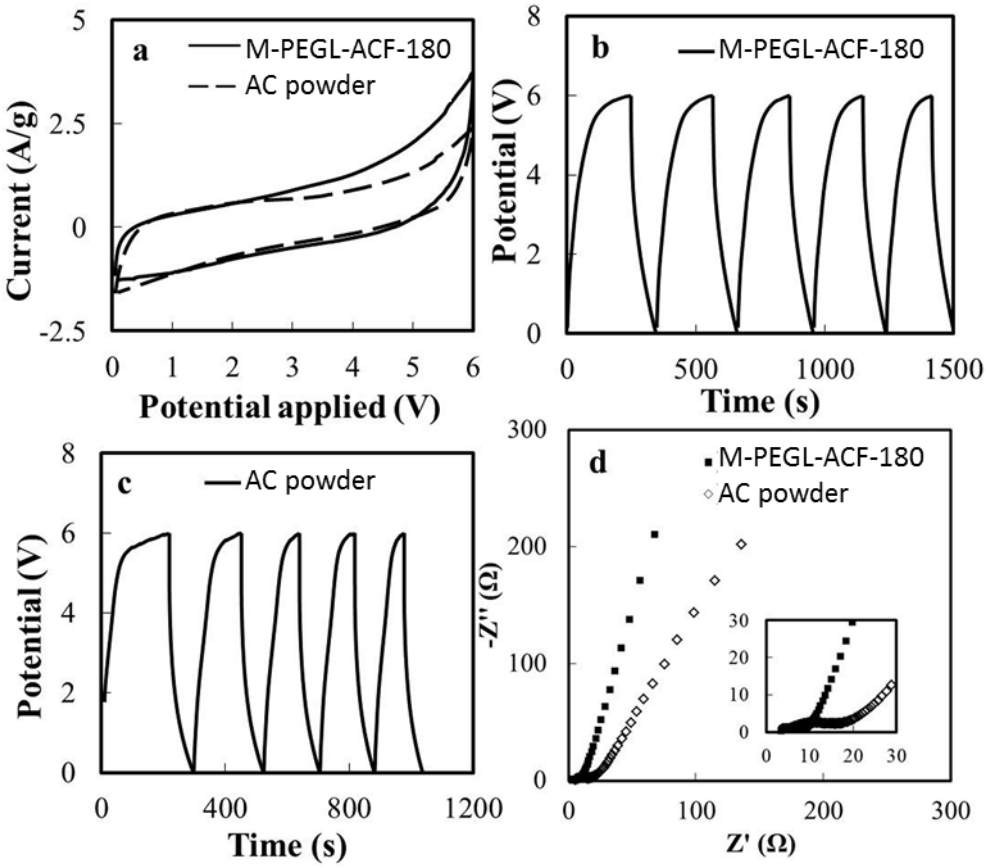

Figure 36. Electrochemical performance of IT-EDLC connected in series: (a) the CV curves of IT-EDLC$_{M\text{-}PEGL\text{-}ACF\text{-}180}$ and IT-EDLC$_{AC\ powder}$ at a scan rate of 0.05 V s^{-1}; (b) the GCD profile of IT-EDLC$_{M\text{-}PEGL\text{-}ACF\text{-}180}$; (c) the GCD profile of IT-EDLC$_{AC\ powder}$ at a current density of 1 A g^{-1}; and (d) the Nyquist plots of IT-EDLC$_{M\text{-}PEGL\text{-}ACF\text{-}180}$ and IT-EDLC$_{AC\ powder}$, where the inset shows magnified profiles of the high frequency range.

If the capacitances of SC-EDLC and the corresponding IT-EDLC are compared, the GCD specific capacitance of IT-EDLC$_{M\text{-}PEGL\text{-}ACF\text{-}180}$ was decreased from 106.9 to 82.0 F g^{-1}

by the series connection. The same tendency was observed for IT-EDLC$_{AC\ powder}$. This may be explained by the following two reasons. One is the increased resistances of the IT-EDLC in series, as shown in **Table 7**. The other is due to the inevitable errors as follows. In the series connection comprising 2 pairs of electrodes or 2 SC-EDLCs, the total capacitance (C_{total}) is expressed as $1/C_{total}=1/C_1 +1/C_2$, where C_1 and C_2 are the capacitances of two SC-EDLCs (Qu and Shi 1998). This equation means that C_{total} is influenced by the lower capacitance of C_1 and C_2. When there is a small difference in the electrode weight of each SC-EDLC, a significant difference in capacitance between each pair of electrodes can be observed. In fact, there were small differences in the weight of the electrodes, although electrodes with a similar weight within 0.1 mg were selected before EDLC assembly. The weight difference may have affected the capacitance of the IT-EDLC with a series connection.

Table 7. Electrochemical performances of EDLCs

Samples	EDLCs connection	Specific capacitance (F g^{-1})[a]	Specific capacitance (F g^{-1})[b]	Intrinsic resistance (Ω)	Charge transfer resistance (Ω)	Energy density (Wh kg^{-1})	Power density (W kg^{-1})	Packaged energy density (Wh kg^{-1})	Packaged power density (W kg^{-1})
M-PEGL-ACF-180	single cell	93.6	106.9	2.3	3.2	33.4	758.8	10.0	280.7
	2 in series	55.5	82.0	3.5	4.4	25.6	931.8	10.3	372.7
	4 in parallel	79.2	102.1	0.8	0.2	31.9	234.8	16.6	122.1
	4 in S/P comb.	94.9	87.3	1.8	2.4	27.3	811.8	14.2	422.1
AC powder	single cell	74.8	65.2	2.4	3.1	20.4	568.6	6.1	210.4
	2 in series	51.0	52.0	5.1	14.5	16.2	742.8	6.5	297.1
	4 in parallel	48.1	60.2	4.0	1.3	18.8	211.8	9.8	110.2
	4 in S/P comb.	81.5	52.6	2.6	2.3	16.4	561.2	8.6	291.8

[a] calculated based on the CV data

[b] calculated based on the GCD profiles

As shown in **Table 7**, IT-EDLC$_{\text{M-PEGL-ACF-180}}$ exhibited an intrinsic resistance (3.5 Ω) and a charge transfer resistance (4.4 Ω) slightly larger than those of SC-EDLC $_{\text{M-PEGL-ACF-180}}$ (2.3 Ω and 3.2 Ω, respectively), suggesting that an efficient lamination was carried out for the series connection. On the other hand, both resistances of IT-EDLC$_{\text{AC powder}}$ were significantly increased, especially the charge transfer resistance (from 3.1 Ω to 14.5 Ω). The large increase in the charge transfer resistance of IT-EDLC$_{\text{AC powder}}$ may result from the small average pore size of the AC powder (1.5 nm) compared with that of M-PEGL-ACF-180 (1.7 nm), which indicated an insufficient penetration of the electrolyte ions into the pores of the electrode. Because of the increase in both of the resistances of IT-EDLC$_{\text{M-PEGL-ACF-180}}$, its energy density was decreased from 33.4 Wh kg^{-1} for SC-EDLC$_{\text{M-PEGL-ACF-180}}$ to 25.6 Wh kg^{-1}. This is caused by complex internal tandem connection. The packaged energy density of IT-EDLC was only slightly increased by the series connection (from 10.0 Wh kg^{-1} to 10.3 Wh kg^{-1}). The enhanced resistance also affected the packaged energy density. However, the packaged power density was dramatically increased by 33%, compared with that of SC-EDLC$_{\text{M-PEGL-ACF-180}}$ (from 280.7 W kg^{-1} to 372.7 W kg^{-1}). Thus, the series connection considerably improved the packaged power density. The same tendency was also observed for IT-EDLC$_{\text{AC powder.}}$

4.2.2 IT-EDLC in parallel connection

Figure 37 shows the electrochemical properties of the IT-EDLCs connected in parallel, which consist of 4 pairs of electrodes. The CV scan rate and the current density of the GCD measurement were identical to those of the above experiments. To elucidate the effects of the parallel connection, the electrochemical properties of parallel-connected.

IT-EDLC$_{M\text{-}PEGL\text{-}ACF\text{-}180}$ were first compared with those of SC-EDLC$_{M\text{-}PEGL\text{-}ACF\text{-}180}$. As with the SC-EDLC, stable CV profiles in a potential window of 0-3 V were obtained. The range of output current for the IT-EDLC in parallel (-8.3 to 7.6 A g^{-1} at 1.5 V) was larger than that of the SC-EDLC (-2.5 to 2.2 A g^{-1} at 1.5 V). In **Table 7,** the specific capacitance of the IT-EDLC based on the weight of electrode was almost the same as that of the SC-EDLC. Because this IT-EDLC had 4 times the number of SC-EDLC electrodes, the total capacitance was also estimated to be 4 times that of the SC-EDLC. The intrinsic and polarization resistances were also decreased by the connection compared with two such EDLCs (**Table 7)**. Thus, the parallel connection gave a large capacitance and output current and low resistances.

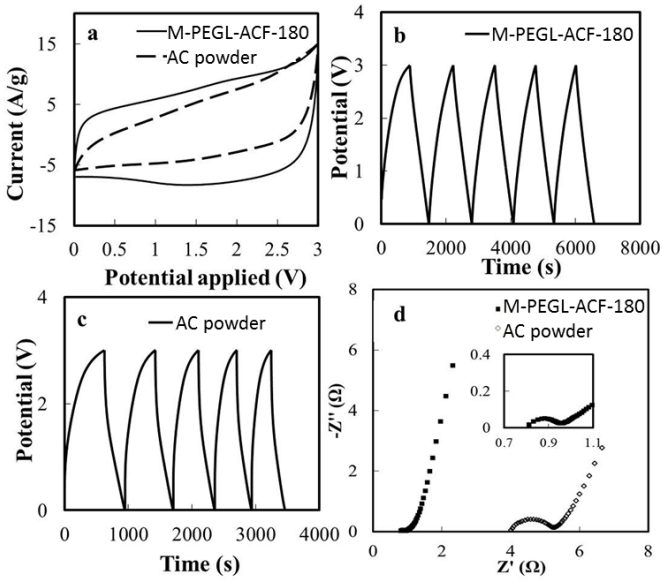

Figure 37. Electrochemical performance of IT-EDLC connected in parallel: (a) the CV curves of IT-EDLC$_{M\text{-}PEGL\text{-}ACF\text{-}180}$ and IT-EDLC$_{AC\ powder}$ at a scan rate of 0.05 V s^{-1}; (b) the GCD profile of IT-EDLC$_{M\text{-}PEGL\text{-}ACF\text{-}180}$; (c) the GCD profile of IT-EDLC$_{AC\ powder}$ at a current density of 1 A g^{-1}; and (d) the Nyquist plots of IT-EDLC$_{M\text{-}PEGL\text{-}ACF\text{-}180}$ and IT-EDLC$_{AC\ powder,}$ where the inset shows the magnified profile of IT-EDLC$_{M\text{-}PEGL\text{-}ACF\text{-}180}$ in the high frequency range.

By such effects, the packaged energy density of IT-EDLC$_{M\text{-}PEGL\text{-}ACF\text{-}180}$ was increased to 16.6 Wh kg^{-1}, which corresponded to 1.66 times that of SC-EDLC$_{M\text{-}PEGL\text{-}ACF\text{-}180}$. However, the packaged power density decreased from 280.7 to 122.1 W kg^{-1}. This phenomenon is similar to the behavior of second batteries (Simon and Gogotsi 2008). When they show a large energy density, the power density becomes low because of its long discharging time.

Similarly, the IT-EDLC$_{AC\ powder}$ also showed the same tendency as IT-EDLC$_{M\text{-}PEGL\text{-}ACF\text{-}180}$ connected in parallel, but the IT-EDLC$_{M\text{-}PEGL\text{-}ACF\text{-}180}$ exhibits a better electrochemical performance than the corresponding IT-EDLC$_{AC\ powder}$.

4.2.3 IT-EDLC in S/P comb. connection

Finally, S/P comb.-connected IT-EDLCs consisting of 4 pairs of electrodes were fabricated to combine the advantages of both series and parallel connections. The same tendencies were observed for both S/P comb.-connected IT-EDLC$_{M\text{-}PEGL\text{-}ACF\text{-}180}$ and IT-EDLC$_{AC\ powder.}$ Here, we explained IT-EDLC$_{M\text{-}PEGL\text{-}ACF\text{-}180}$ as an example. The IT-EDLC$_{M\text{-}PEGL\text{-}ACF\text{-}180}$ showed a stable CV profile in a doubled potential window (0-6 V) similar to that obtained with a series connection. Its range of output current (-1.7 to 3.1 A g^{-1} at 3 V) was almost identical to SC-EDLC$_{M\text{-}PEGL\text{-}ACF\text{-}180}$. The Nyquist plot in **Figure 38d** shows that IT-EDLC$_{M\text{-}PEGL\text{-}ACF\text{-}180}$ has an intrinsic resistance of 1.8 Ω and a charge transfer resistance of 2.4 Ω.

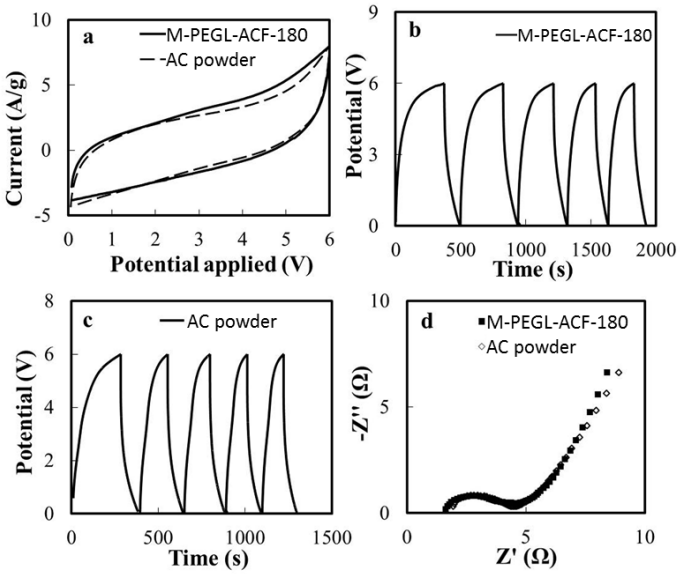

Figure 38. Electrochemical performance of IT-EDLC connected in the S/P comb.: (a) the CV curves of IT-EDLC$_{\text{M-PEGL-ACF-180}}$ and IT-EDLC$_{\text{AC powder}}$ at a scan rate of 0.05 V s^{-1}; (b) the GCD profile of IT-EDLC$_{\text{M-PEGL-ACF-180}}$; (c) the GCD profile of IT-EDLC$_{\text{AC powder}}$ at a current density of 2 A g^{-1}; and (d) the Nyquist plots of IT-EDLC$_{\text{M-PEGL-ACF-180}}$ and IT-EDLC$_{\text{AC powder}}$.

In general, a higher current density gives a lower specific capacitance (El-Kady et al., 2012). However, it took a very long time for IT-EDLC$_{\text{M-PEGL-ACF-180}}$ to discharge at the current density previously used of 1 A g^{-1}. Therefore, the GCD measurement was carried out at 2 A g^{-1} to confirm its repeatability. The specific capacitance of the S/P comb.-connected IT-EDLC$_{\text{M-PEGL-ACF-180}}$ was found to be 87.3 F g^{-1}, which was larger than that of the series-connected IT-EDLC$_{\text{M-PEGL-ACF-180}}$ but smaller than that of the parallel-connected one. Generally, the resistances are increased with the series connection, whereas they are decreased with the parallel connection. Accordingly, the higher specific capacitance was caused by an effect of the parallel connection.

Based on the specific capacitance, the packaged energy density and power density of the

IT-EDLC$_{M\text{-}PEGL\text{-}ACF\text{-}180}$ were calculated to be 14.2 Wh kg^{-1} and 422.1 W kg$^{-1,}$ respectively. They were remarkably larger than those of SC-EDLC$_{M\text{-}PEGL\text{-}ACF\text{-}180}$. Therefore, both the energy and the power densities of the package were improved by the S/P comb. connection.

Chapter 5 Conclusions

This study was conducted to develop electrode for electric double layer capacitor (EDLC) from three kinds of isolated lignins as a novel value-added application of lignins, and to achieve the following three objectives: 1) to prepare lignin-based activated carbon fibers (ACFs) from the lignins, hardwood acetic acid lignin (HAL), polyethylene glycol lignin (PEGL) and soda lignin (SL); 2) to assemble single cell type EDLCs (SC-EDLCs) with resultant ACFs with different electrolytes; 3) to develop internal tandem EDLCs (IT-EDLCs) with high electrochemical performance, such high energy density and high power density, by using a direct lamination of single side- and double sides-coated electrodes.

Here, I summarize the achievements of doctoral thesis research according to the above objectives.

1) Preparation of lignin-based ACFs

A process of ACFs production consisted of spinning, thermostabilization, carbonization and activation. As a first step, lignin fibers were successfully prepared from HAL, PEGL and SL by means of electrospinning and melt spinning methods. The fabricated lignin fibers showed small diameters in the range from 0.85 μm to 37.7 μm. Especially, the electrospinning gave fine fibers with diameters of 0.85 – 5.17 μm.

The thermostabilization was a key step to fabricate lignin-based ACFs, because without thermostabilization, the resultant lignin fibers were melted or deformed at an elevated temperature during the following carbonization process. Therefore, the thermostabilization was required to suppress the deformation of lignin fibers. Unfortunately, a conventional oxidative thermostabilization with air as a crosslinker of lignin molecules was

found to be unsuitable for electrospun HAL and PEGL fibers, because it took a very long time (about 38 h) to completely fabricate infusible fibers. Thereby, formaldehyde, which was generated by adding hexamine into acidic lignin solution before electrospinning, was introduced to crosslink lignin molecules to improve the thermostability of the fibers. This developed newly method required only 3 h for the complete conversion of the HAL and PEGL fibers to infusible ones. In addition, melt spun PEGL fibers could be transformed to infusible ones by the combination of chemical treatment to cleave PEG moiety from PEGL and a conventional oxidative thermostabilization. This process was also completed within 3 h in total. On the other hand, electrospun SL fibers were easily thermostabilized by the conventional method within 3 h. This result indicated that SL was more thermally stable than other isolated lignins. In fact, melt spinning of SL was impossible to carry out.

Thus, I established thermostabilization processes for all lignin fibers, which were completed with 3 h. The resultant thermostabilized fibers were, in turn, subjected to carbonization and activation.

After carbonization and activation, thin ACFs (diameters ranging from 270 nm to 20.6 μm) with large surface area and different pore size distributions were finally fabricated. N_2 adsorption/desorption analysis revealed that BET specific surface areas of most ACFs samples were larger than 2000 $m^2\ g^{-1}$. This value was much larger than that of commercially available AC (1434 $m^2\ g^{-1}$). The analysis also revealed that micro/mesopores, as an adsorption site, largely contributed to the total surface area of the lignin-based ACFs, while macropores as a transport domain of adsorption were responsible for that of commercial AC.

2) To assemble single cell type EDLCs (SC-EDLCs) with lignin-based ACFs with different electrolytes

SC-EDLCs were assembled with the prepared ACFs as major electrode constituents and organic/aqueous electrolytes. In the organic electrolyte system ($TEMABF_4$/PC), the SC-EDLC derived from E-HAL-ACF-105 showed the highest specific capacitance of 133.3 F g^{-1} at the current density of 1 A g^{-1} among all SC-EDLCs assembled with all ACFs, whose value was twice that of SC-EDLC from commercial AC powder (65.2 F g^{-1}). However, the capacitance of SC-EDLC derived from E-HAL-ACF-180 was decreased to 63.5 F g^{-1}. The superior performance of the $EDLC_{E\text{-}HAL\text{-}ACF\text{-}105}$ was attributed to their large BET surface area and abundant meso- and micropores. However, such small pores of E-HAL-ACF-105 brought about slightly large charge transfer resistance of 12.0 Ω. Similarly, M-PEGL-ACF-180, which has large surface area rich in micro- and mesopores, also showed a high capacitance of 109.5 F g^{-1}. In this case, however, the charge transfer resistance was very small (3.2 Ω). On the other hand, when using an aqueous electrolyte (6M KOH), the resultant SC-EDLC with ACFs from electrospun PEGL fibers exhibited a capacitance of 121.2 F g^{-1}. Interstingly, the value was lower than that from commercial AC powder (140.2 F g^{-1}). This difference would be attributed to the difference in pore composition.

3) To develop internal tandem EDLCs (IT-EDLCs)

To improve electrochemical performance of lignin-based EDLC based on the package weight, three types of IT-EDLCs were fabricated by direct laminations of single- and double-side coated electrodes comprised of M-PEGL-ACF-180 as a major electrode constituent. By the series connection, the packaged power density (372.7 W kg^{-1}) was

significantly increased, whereas the packaged energy density was not changed. By the parallel connection, the packaged energy density was remarkably increased, but the packaged power density was decreased. With a combination of series and parallel connections, the EDLC possessed both a high packaged power density (422.1 W kg^{-1}) and packaged energy density (14.2 Wh kg^{-1}). These alternations for the electrochemical performance of EDLC upon the series, parallel and their combination connections were very reasonable from the viewpoint of electricity. Thus, by using the internal tandem lamination of electrodes, I successfully assembled the EDLC with a large electrostatic capacitance and a wide potential window.

General discussion

Lignin has drawn much attention as an effectively unused biomass component since the last century, because lignin as a by-product of pulping industry is merely burned for energy recovery after concentration of the black liquor, although it is an abundant aromatic polymer with high carbon content on earth. Its use in other applications, such as dispersants, resins and adhesives, has been investigated. However, these are not necessarily considered to be high value-added materials. As a result, development of more value-added materials from lignin is an important research subject in order to promote lignin utilization. From this viewpoint, I prepared ACFs from several isolated lignins, and attempted to apply them to electrodes for EDLC. ACFs, which are called as fibrous activated carbon, have already been focused on as the most excellent adsorbent among activated carbons with various shapes. Especially, ACFs with large specific BET surface area are remarkably required and

consumed, although they are expensive. I consider that ACFs production with large surface area from electrospun and melt-spun fibers exploit a novel way to their fabrication as an adsorbent. Furthermore, this study demonstrated to assemble SC-EDLCs with lignin-based ACFs, and their electrochemical performance in relation to the pore composition in ACFs and the interaction of ACFs with the electrolytes used. I am convinced that achievements and findings of this research contribute not only to a new application of lignin, but also to the development of lignin-based EDLC with further improved electrochemical performance. Taking into consideration the sustainable supply of lignin as a by-product in paper industry, a study on lignin, in terms of structure, reactivity and applications, is still promising, and is expected to be further developed.

References

Aso T, Koda K, Kubo S, Yamada T, Nakajima I, Uraki Y (2013) Preparation of Novel Lignin-Based Cement Dispersants from Isolated Lignins. J Wood Chem Technol 33: 286-298

Ayutsede J, Gandhi M, Sukigara S, Micklus M, Chen H-E, Ko F (2005) Regeneration of Bombyx mori silk by electrospinning. Part 3: characterization of electrospun nonwoven mat. Polymer 46: 1625-1634

Baker DA, Gallego NC, Baker FS (2012) On the characterization and spinning of an organic-purified lignin toward the manufacture of low-cost carbon fiber. J Appl Polym Sci 124: 227-234

Beachley V, Wen X (2009) Effect of electrospinning parameters on the nanofiber diameter and length. Materials Science and Engineering: C 29: 663-668

Binh NTT, Luong ND, Kim DO, Lee SH, Kim BJ, Lee YS, Nam JD (2009) Synthesis of Lignin-Based Thermoplastic Copolyester Using Kraft Lignin as a Macromonomer. Compos Interfaces 16: 923-935

Bozell JJ, Petersen GR (2010) Technology development for the production of biobased products from biorefinery carbohydrates-the US Department of Energy's "Top 10" revisited. Green Chem 12: 539-554

Braun J, Holtman K, Kadla J (2005) Lignin-based carbon fibers: Oxidative thermostabilization of kraft lignin. Carbon 43: 385-394

Calvo-Flores FG, Dobado JA (2010) Lignin as renewable raw material. ChemSusChem 3: 1227-1235

Chand S (2000) Review carbon fibers for composites. Journal of Materials Science 35: 1303-1313

Chen J-P, Chang G-Y, Chen J-K (2008) Electrospun collagen/chitosan nanofibrous membrane as wound dressing. Colloids Surf, A 313–314: 183-188

Chen W, Xia C, Alshareef H (2015) Graphene based integrated tandem supercapacitors fabricated directly on separators. Nano Energy 15: 1-8

Ciobanu C, Ungureanu M, Ignat L, Ungureanu D, Popa VI (2004) Properties of lignin–polyurethane films prepared by casting method. Ind Crops Prod 20: 231-241

Dallmeyer I, Ko F, Kadla JF (2010) Electrospinning of Technical Lignins for the Production of Fibrous Networks. J Wood Chem Technol 30: 315-329

Davies A, Yu A (2011) Material advancements in supercapacitors: From activated carbon to carbon nanotube and graphene. The Canadian Journal of Chemical Engineering 89: 1342-1357

El-Kady MF, Strong V, Dubin S, Kaner RB (2012) Laser scribing of high-performance and flexible graphene-based electrochemical capacitors. Science 335: 1326-1330

Endo M, Maeda T, Takeda T, Kim YJ, Koshiba K, Hara H, Dresselhaus MS (2001) Capacitance and Pore-Size Distribution in Aqueous and Nonaqueous Electrolytes Using Various Activated Carbon Electrodes. J Electrochem Soc 148: A910-A914

Faruk O, Sain M (2015) Lignin in Polymer Composites. Elsevier Science

Fitzer E, Müller DJ (1975) The influence of oxygen on the chemical reactions during stabilization of pan as carbon fiber precursor. Carbon 13: 63-69

Frank E, Hermanutz F, Buchmeiser MR (2012) Carbon Fibers: Precursors, Manufacturing,

and Properties. Macromol Mater Eng 297: 493-501

Gandini A (2008) Polymers from Renewable Resources: A Challenge for the Future of Macromolecular Materials. Macromolecules 41: 9491-9504

Gellerstedt G, Henriksson G (2008) Chapter 9 - Lignins: Major Sources, Structure and Properties. *In* B Mohamed Naceur, G Alessandro, eds, Monomers, Polymers and Composites from Renewable Resources. Elsevier, Amsterdam, pp 201-224

Gogotsi Y, Simon P (2011) True Performance Metrics in Electrochemical Energy Storage. Science 334: 917-918

Gosselink R, De Jong E, Guran B, Abächerli A (2004) Co-ordination network for lignin—standardisation, production and applications adapted to market requirements (EUROLIGNIN). Ind Crops Prod 20: 121-129

Gryglewicz G, Machnikowski J, Lorenc-Grabowska E, Lota G, Frackowiak E (2005) Effect of pore size distribution of coal-based activated carbons on double layer capacitance. Electrochim Acta 50: 1197-1206

Gupta P, Elkins C, Long TE, Wilkes GL (2005) Electrospinning of linear homopolymers of poly(methyl methacrylate): exploring relationships between fiber formation, viscosity, molecular weight and concentration in a good solvent. Polymer 46: 4799-4810

Homma H, Kubo S, Yamada T, Koda K, Matsushita Y, Uraki Y (2010) Conversion of Technical Lignins to Amphiphilic Derivatives with High Surface Activity. J Wood Chem Technol 30: 164-174

Hu M, Sui S, Zhu X, Yu Q, Cao G, Hong X, Tu H (2006) A 10kW class PEM fuel cell stack based on the catalyst-coated membrane (CCM) method. Int J Hydrogen Energy 31:

1010-1018

Huang Z-M, Zhang YZ, Kotaki M, Ramakrishna S (2003) A review on polymer nanofibers by electrospinning and their applications in nanocomposites. Compos Sci Technol 63: 2223-2253

Inagaki M, Konno H, Tanaike O (2010) Carbon materials for electrochemical capacitors. J Power Sources 195: 7880-7903

Jiang Z, Tai D, Lee Z (1991) Characterization of Residual Lignin in Alkaline Pulp of Wheat Straw. China Pulp & Paper 1: 009

Jieying Z, Zhao Q, Ye Z (2014) Preparation and characterization of activated carbon fiber (ACF) from cotton woven waste. Appl Surf Sci 299: 86-91

Johansson A, Aaltonen O, Ylinen P (1987) Organosolv pulping — methods and pulp properties. Biomass 13: 45-65

Kadla JF, Kubo S, Venditti RA, Gilbert RD, Compere AL, Griffith W (2002) Lignin-based carbon fibers for composite fiber applications. Carbon 40: 2913-2920

Kaneko K (1994) Determination of pore size and pore size distribution: 1. Adsorbents and catalysts. J Membr Sci 96: 59-89

Kim T, Jung G, Yoo S, Suh KS, Ruoff RS (2013) Activated Graphene-Based Carbons as Supercapacitor Electrodes with Macro- and Mesopores. ACS Nano 7: 6899-6905

Ko F, Gogotsi Y, Ali A, Naguib N, Ye H, Yang GL, Li C, Willis P (2003) Electrospinning of Continuous Carbon Nanotube-Filled Nanofiber Yarns. Adv Mater 15: 1161-1165

Kubo S, Kadla JF (2004) Poly(Ethylene Oxide)/Organosolv Lignin Blends: Relationship between Thermal Properties, Chemical Structure, and Blend Behavior.

Macromolecules 37: 6904-6911

Kubo S, Kadla JF (2005) Lignin-based Carbon Fibers: Effect of Synthetic Polymer Blending on Fiber Properties. J Polym Environ 13: 97-105

Kubo S, Uraki Y, Sano Y (1998) Preparation of carbon fibers from softwood lignin by atmospheric acetic acid pulping. Carbon 36: 1119-1124

Li M, Mondrinos MJ, Gandhi MR, Ko FK, Weiss AS, Lelkes PI (2005) Electrospun protein fibers as matrices for tissue engineering. Biomaterials 26: 5999-6008

Lin C-K, Huang L-H, Chiang L-K, Chyou Y-P (2009) Thermal stress analysis of planar solid oxide fuel cell stacks: effects of sealing design. J Power Sources 192: 515-524

Lin J, Koda K, Kubo S, Yamada T, Enoki M, Uraki Y (2013) Improvement of Mechanical Properties of Softwood Lignin-Based Carbon Fibers. J Wood Chem Technol 34: 111-121

Lin J, Kubo S, Yamada T, Koda K, Uraki Y (2012) Chemical thermostabilization for the preparation of carbon fibers from softwood lignin. BioResources 7: 5634-4646

Liu CL, Dong WS, Cao GP, Song JR, Liu L, Yang YS (2008) Capacitance limits of activated carbon fiber electrodes in aqueous electrolyte. J Electrochem Soc 155: F1-F7

Mansouri N-EE, Salvadó J (2006) Structural characterization of technical lignins for the production of adhesives: Application to lignosulfonate, kraft, soda-anthraquinone, organosolv and ethanol process lignins. Ind Crops Prod 24: 8-16

Mansouri NEE, Pizzi A, Salvado J (2007) Lignin‐based polycondensation resins for wood adhesives. J Appl Polym Sci 103: 1690-1699

Martin C, Ronda JC, Cadiz V (2006) Development of novel flame-retardant thermosets based on boron-modified phenol-formaldehyde resins. Journal of Polymer Science Part a-Polymer Chemistry 44: 3503-3512

Mathiasson A, Kubat DG (1994) Lignin as Binder in Particle Boards Using High-Frequency Heating - Properties and Modulus Calculations. Holz Als Roh-Und Werkstoff 52: 9-18

Matthews JA, Wnek GE, Simpson DG, Bowlin GL (2002) Electrospinning of Collagen Nanofibers. Biomacromolecules 3: 232-238

Montane D, Farriol X, Salvado J, Jollez P, Chornet E (1998) Application of steam explosion to the fractionation and rapid vapor-phase alkaline pulping of wheat straw. Biomass Bioenergy 14: 261-276

Norris ID, Shaker MM, Ko FK, MacDiarmid AG (2000) Electrostatic fabrication of ultrafine conducting fibers: polyaniline/polyethylene oxide blends. Synth Met 114: 109-114

Pandolfo A, Hollenkamp A (2006) Carbon properties and their role in supercapacitors. J Power Sources 157: 11-27

Pham QP, Sharma U, Mikos AG (2006) Electrospinning of polymeric nanofibers for tissue engineering applications: a review. Tissue Eng 12: 1197-1211

Pouteau C, Baumberger S, Cathala B, Dole P (2004) Lignin–polymer blends: evaluation of compatibility by image analysis. CR Biol 327: 935-943

Qu D, Shi H (1998) Studies of activated carbons used in double-layer capacitors. J Power Sources 74: 99-107

Rajalakshmi N, Pandiyan S, Dhathathreyan K (2008) Design and development of modular

fuel cell stacks for various applications. Int J Hydrogen Energy 33: 449-454

Ramakrishna S, Fujihara K, Teo W-E, Lim T-C, Ma Z (2005) Introduction. *In* An Introduction To Electrospinning And Nanofibers. WORLD SCIENTIFIC, pp 1-21

Reneker DH, Yarin AL (2008) Electrospinning jets and polymer nanofibers. Polymer 49: 2387-2425

Rodríguez A, Moral A, Serrano L, Labidi J, Jiménez L (2008) Rice straw pulp obtained by using various methods. Bioresour Technol 99: 2881-2886

Salitra G, Soffer A, Eliad L, Cohen Y, Aurbach D (2000) Carbon Electrodes for Double‐Layer Capacitors I. Relations Between Ion and Pore Dimensions. J Electrochem Soc 147: 2486-2493

Shi H (1996) Activated carbons and double layer capacitance. Electrochim Acta 41: 1633-1639

Simon P, Burke A (2008) Nanostructured carbons: double-layer capacitance and more. The electrochemical society interface 17: 38

Simon P, Gogotsi Y (2008) Materials for electrochemical capacitors. Nat Mater 7: 845-854

Stewart D (2008) Lignin as a base material for materials applications: Chemistry, application and economics. Ind Crops Prod 27: 202-207

Sudo K, Shimizu K (1992) A new carbon fiber from lignin. J Appl Polym Sci 44: 127-134

Suzuki M (1994) Activated carbon fiber: Fundamentals and applications. Carbon 32: 577-586

Tian XC, Shi MZ, Xu X, Yan MY, Xu L, Minhas-Khan A, Han CH, He L, Mai LQ (2015) Arbitrary Shape Engineerable Spiral Micropseudocapacitors with Ultrahigh Energy

and Power Densities. Adv Mater 27: 7476-7482

Tsai PP, Schreuder-Gibson H, Gibson P (2002) Different electrostatic methods for making electret filters. J Electrostat 54: 333-341

Uraki Y, Kubo S, Kurakami H, Sano Y (1997) Activated Carbon Fibers from Acetic Acid Lignin. Holzforschung 51: 188-192

Uraki Y, Kubo S, Nigo N, Sano Y, Sasaya T (1995) Preparation of Carbon Fibers from Organosolv Lignin Obtained by Aqueous Acetic Acid Pulping. Holzforschung 49: 343-350

Uraki Y, Nakatani A, Kubo S, Sano Y (2001) Preparation of activated carbon fibers with large specific surface area from softwood acetic acid lignin. Journal of Wood Science 47: 465-469

Voitl T, Rohr PRv (2009) Demonstration of a Process for the Conversion of Kraft Lignin into Vanillin and Methyl Vanillate by Acidic Oxidation in Aqueous Methanol. Industrial & Engineering Chemistry Research 49: 520-525

Wang C, Appleby AJ, Little FE (2001) Electrochemical impedance study of initial lithium ion intercalation into graphite powders. Electrochim Acta 46: 1793-1813

Wang G, Zhang L, Zhang J (2012) A review of electrode materials for electrochemical supercapacitors. Chem Soc Rev 41: 797-828

Wikipedia contributors (2016a) "Electrolysis of water", Wikipedia, The Free Encyclopedia. https://en.wikipedia.org/w/index.php?title=Electrolysis_of_water&oldid=722257540

Wikipedia contributors (2016b) "Lignin", Wikipedia, The Free Encyclopedia. https://en.wikipedia.org/wiki/Lignin

You X, Duan J, Koda K, Yamada T, Uraki Y (2015a) Preparation of electric double layer capacitors (EDLCs) from two types of electrospun lignin fibers. Holzforschung. DOI: 10.1515/hf-2015-0175 (*In press)*

You X, Koda K, Yamada T, Uraki Y (2015b) Preparation of electrode for electric double layer capacitor from electrospun lignin fibers. Holzforschung 69: 1097-1106

Zhang F, Lu YH, Yang X, Zhang L, Zhang TF, Leng K, Wu YP, Huang Y, Ma YF, Chen YS (2014) A Flexible and High-Voltage Internal Tandem Supercapacitor Based on Graphene-Based Porous Materials with Ultrahigh Energy Density. Small 10: 2285-2292

Zhang LL, Zhao XS (2009) Carbon-based materials as supercapacitor electrodes. Chem Soc Rev 38: 2520-2531

Acknowledgements

I would like to express my gratitude and appreciation for the many people that have guided me throughout my Doctoral study. First, I would like to thank my supervisor, Prof. Yasumitsu Uraki, for giving me the opportunity to study in this outstanding group. His rigorous attitude in doing research has strongly affected me and will continue to do so throughout my further life. I would also like to thank Dr. Keiichi Koda, who has provided helpful advice and constructive criticism. This project could not be completed successfully without the guidance and assistance from both of them

I am also very thankful to all my lab members, who are always helping me with great kindness when I have problem in experiment, and accompany with me in the 5 years' happy study in Japan. Great thanks are also to our department faculty, staff, and fellow students for their friendship and help.

I would like to dedicate this thesis work to my wife, my parents and other family members who have continuously provided me with love, patience, and support.